Regular Article

LYMPHOID NEOPLASIA

An animal model of adult T-cell leukemia: humanized mice with HTLV-1–specific immunity

Kenta Tezuka, Runze Xun, Mami Tei, Takaharu Ueno, Masakazu Tanaka, Norihiro Takenouchi, and Jun-ichi Fujisawa

Department of Microbiology, Kansai Medical University, Hirakata, Osaka, Japan

Key Points

- Humanized mice, IBMI-huNOG, were generated by intra–bone marrow injection of human CD133$^+$ hematopoietic stem cells.
- HTLV-1–infected IBMI-huNOG mice recapitulated distinct ATL-like symptoms as well as HTLV-1–specific adaptive immune responses.

Human T-cell leukemia virus type 1 (HTLV-1) is causally associated with adult T-cell leukemia (ATL), an aggressive T-cell malignancy with a poor prognosis. To elucidate ATL pathogenesis in vivo, a variety of animal models have been established; however, the mechanisms driving this disorder remain poorly understood due to deficiencies in each of these animal models. Here, we report a novel HTLV-1–infected humanized mouse model generated by intra–bone marrow injection of human CD133$^+$ stem cells into NOD/Shi-scid/IL-2Rγc null (NOG) mice (IBMI-huNOG mice). Upon infection, the number of CD4$^+$ human T cells in the periphery increased rapidly, and atypical lymphocytes with lobulated nuclei resembling ATL-specific flower cells were observed 4 to 5 months after infection. Proliferation was seen in both CD25$^-$ and CD25$^+$ CD4 T cells with identical proviral integration sites; however, a limited number of CD25$^+$-infected T-cell clones eventually dominated, indicating an association between clonal selection of infected T cells and expression of CD25. Additionally, HTLV-1–specific adaptive immune responses were induced in infected mice and might be involved in the control of HTLV-1–infected cells. Thus, the HTLV-1–infected IBMI-huNOG mouse model successfully recapitulated the development of ATL and may serve as an important tool for investigating in vivo mechanisms of ATL leukemogenesis and evaluating anti-ATL drug and vaccine candidates. (*Blood.* 2014;123(3):346-355)

Introduction

Human T-cell leukemia virus type 1 (HTLV-1) is a retrovirus associated with adult T-cell leukemia (ATL) and HTLV-1–associated myelopathy or tropical spastic paraparesis (HAM/TSP) in humans.[1-3] Although the majority of HTLV-1–infected individuals remain asymptomatic throughout their lives, approximately 5% of HTLV-1 carriers develop ATL or HAM/TSP following a long latency period.[4] In addition to the classic structural proteins required for retroviral replication, the HTLV-1 proviral genome encodes several accessory and regulatory proteins, including the viral transcriptional activator Tax and the HTLV-1 bZIP factor (HBZ), which are thought to be linked to HTLV-1 pathogenesis.[5,6]

ATL is an aggressive malignancy of mature CD4 T cells, characterized by frequent visceral involvement, lymphadenopathy, hypercalcemia or hypercytokinemia, and monoclonal proliferation of HTLV-1–infected tumor cells.[7] Typical ATL cells exhibit an unusual morphology with lobulated nuclei, known as "flower cells."[8] These cells are also characterized by their robust expression of interleukin (IL)-2 receptor α (CD25).[9]

To reproduce the pathogenesis of ATL, a number of mouse models have been developed, including transgenic or xenografted/humanized mice.[10-18] One such model is the Tax-transgenic mouse, which expresses Tax under the control of the Lck promoter. This model restricts Tax expression to developing thymocytes, resulting in characteristic ATL-like phenotypes.[15] Another model, the HBZ-transgenic mouse, expresses HBZ under the control of a CD4-specific promoter/enhancer/silencer. These mice develop lymphomas characterized by induction of Foxp3 in CD4 T cells, similar to leukemic cells in ATL patients.[18] These observations clearly demonstrate that the leukemogenic activity of not only Tax but also HBZ is related to the development of ATL.

In addition to transgenic mouse models, a variety of HTLV-1–infected small-animal models have been established to evaluate viral pathogenesis and elucidate the function of viral products in vivo.[19,20] These infection models have provided valuable findings regarding virus-host interactions; however, they are unable to fully recapitulate pathological conditions resembling ATL, likely due to the low efficiency of HTLV-1 infection.

Humanized mice are highly susceptible to infection with human lymphotropic viruses such as EBV, HIV-1, and HTLV-1, and have been used to recapitulate specific disorders and human immune responses.[17,21,22] Recent studies on HTLV-1 infection in humanized mouse models successfully reproduced HTLV-1–associated T-cell lymphomas[16,17]; however, these models did not accurately recreate human immune responses against HTLV-1.

Submitted June 17, 2013; accepted October 27, 2013. Prepublished online as *Blood* First Edition paper, November 6, 2013; DOI 10.1182/blood-2013-06-508861.

The online version of this article contains a data supplement.

There is an Inside *Blood* commentary on this article in this issue.

The publication costs of this article were defrayed in part by page charge payment. Therefore, and solely to indicate this fact, this article is hereby marked "advertisement" in accordance with 18 USC section 1734.

Notably, humoral immunity, along with cytotoxic T cell (CTL)-mediated cytotoxicity, is thought to play a pivotal role in controlling the proliferation or selection of HTLV-1–infected T-cell clones in vivo.[23,24] It is therefore important to develop mouse models of ATL that induce more human-like HTLV-1–specific immune responses.

In this study, we describe a novel humanized mouse model of HTLV-1 infection in the presence of specific adaptive immune responses. Our novel HTLV-1–infected humanized mice displayed distinct ATL-like symptoms, including hepatosplenomegaly, hypercytokinemia, oligoclonal proliferation of HTLV-1–infected T cells, and the appearance of flower cells. In addition, HTLV-1–specific immunity was induced and may be involved in the control of infected cells in vivo.

Materials and methods

Purification of human CD133$^+$ cells from cord blood

Cord blood samples from full-term human deliveries were obtained from the Japanese Red Cross Kinki Cord Blood Bank (Osaka, Japan) for research use due to the inadequate numbers of stem cells for human transplantation; all patients provided signed, informed consent in accordance with the Declaration of Helsinki. Mononuclear cells (MNCs) were separated using Ficoll-Conray (Lymphosepar I, IBL) density gradient centrifugation. After collecting MNCs, a CD133 MicroBead Kit (Miltenyi Biotec) was used to isolate human CD133$^+$ cells (Miltenyi Biotec) according to the manufacturer's instructions. HLA-A typing was performed using a WAKFlow HLA typing kit (WAKUNAGA) according to the manufacturer's instructions; the results are shown in supplemental Table 1 (available on the *Blood* Web site).

NOG mice

Female 6-week-old NOD/Shi-scid/IL-2Rγc null (NOG) mice[25] were purchased from the Central Institute of Experimental Animals (Kawasaki, Japan). Mice were handled under sterile conditions and were maintained in germ-free isolators. All animal experiments were approved by the Animal Care Committees of Kansai Medical University.

Generation of IBMI-huNOG

Seven-week-old NOG mice were sublethally irradiated with 250 cGy from a ^{137}Cs source (Gammacell 40 exactor, Nordion International). Within 24 hours of irradiation, each mouse was injected with 5×10^4 human CD133$^+$ cells by intra–bone marrow injection (IBMI)[26] as reported previously.[27]

HTLV-1 infection to IBMI-huNOG

The HTLV-1–infected T-cell line MT2[28] was irradiated with 10 Gy from a ^{137}Cs source irradiator. Irradiated MT2 cells (2.5×10^6) or phosphate-buffered saline were inoculated intraperitoneally into 24- to 28-week-old IBMI-huNOG mice. Mice were anesthetized and killed when the body weight decreased to <70% of their maximum weight. Peripheral blood smears were prepared using May-Grunwald Giemsa staining and examined by light microscopy. All infections were performed in a Biosafety Level P2A laboratory in accordance with the guidelines of Kansai Medical University.

Flow cytometric analysis and cell sorting

Peripheral blood cells were routinely collected every 2 weeks after infection, and after sacrificing mice, single-cell suspensions of various lymphoid tissues were prepared as described previously.[29] To stain surface markers, anti–human CD45-PerCP or APC-Cy7, CD3–fluorescein isothiocyanate (FITC) or phycoerythrin (PE)-Cy7, CD4-PE, CD8-PerCP-Cy5.5, CD19-PE, CD25-FITC, CCR4-APC antibodies were used, along with mouse immunoglobllin G1 and FITC as an isotype control (all BD Biosciences). AccuCount Ultra Rainbow Fluorescent Particles (Spherotech) were employed to determine absolute cell numbers, according to the manufacturer's protocol. Flow cytometric analysis was performed on a BD FACSCan for 3-color staining and a BD FACSCant II (BD Biosciences) for 7-color staining. The CellQuest and Diva software programs were used for data acquisition (BD Biosciences), and the collected data were analyzed by FCS express 3 (De Novo Software). Human CD4-, CD8-, and CD25-expressing T cells were sorted from splenic MNCs by FACSAria or FACSAria III (BD Biosciences).

Tetramer staining

PE-conjugated HLA-A*24:02/Tax301-309 (SFHSLHLLF) and HLA-A*24:02/HIV (RYLRDQQLL) env gp160 tetramers were purchased from MBL. Splenocytes from mock-infected or HTLV-1–infected mice were stained with each tetramer and anti–human CD3 and CD8 antibodies according to the manufacturer's protocol. Mixed lymphocyte-peptide cultures were performed to stimulate Tax-specific CTLs, as described previously.[30] Briefly, splenocytes from HTLV-1–infected mice were cultured for 13 days with 10 mg/mL Tax301-309 peptide and 50 U/mL recombinant human IL-2 (Takeda Chemical Industries). Cultured splenocytes were then analyzed by flow cytometry.

DNA isolation and quantification of proviral load

Genomic DNA was extracted from single-cell suspensions of tissue or peripheral blood using a conventional phenol extraction method. Proviral loads (PVLs) were measured by quantitative polymerase chain reaction (PCR) using a MyiQ or CFX96 real-time PCR system (Bio-Rad). The primers and probes targeting for HTLV-1 *pX* and human β-globin (HBB; as a internal control) are listed in supplemental Table 2. A plasmid containing PCR fragments for the HTLV-1 *pX* region and HBB was constructed using T-Vector pMD20 (TaKaRa) and used as the quantified standard template for real-time PCR.[31] The PVL was calculated as: [(copy number of *pX*)/(copy number of HBB / 2)] × 100.

Quantification of clonal occupancy by clone-specific PCR

Inverse long PCR (IL-PCR) was performed to amplify the genomic DNA flanked the 3′ long terminal repeat of HTLV-1 provirus according to a modified method described previously.[32] In brief, the genomic DNA was digested by *Pst*I, self-ligated by T4 ligase, and then digested by *Mlu*I. Long PCR amplification of the linearized DNA was performed using the PrimeSTAR GXL DNA polymerase (TaKaRa) according to the manufacturer's protocol. Primer sets for IL-PCR analysis are listed in supplemental Table 3. IL-PCR products were isolated from agarose gels, purified, and subjected to nested PCR. Amplified nested PCR fragments were subcloned into T-Vector pMD20 (TaKaRa) and sequenced to obtain provirus integration sites downstream of the 3′ long terminal repeat. Integration site-specific primers were designed based on the DNA sequence of the flanking region of the provirus derived from splenic DNA of 8 HTLV-1–infected mice, and are listed in supplemental Table 5. A detailed description of the clone-specific quantitative PCR procedure has been provided elsewhere.[33] The clonal occupancy of each clone was calculated as: [(copy number of integration sites)/(copy number of *pX*)] × 100.

Real-time RT-PCR to quantify *tax* and *HBZ* transcripts

Total RNA was isolated using the TRIzol reagent (Invitrogen) and complementary DNA samples were synthesized from 1 μg total RNA. Reverse-transcription PCR (RT-PCR) was performed by the use of SsoFast EvaGreen Supermix (Bio-Rad). Primers used for RT-PCR are listed in supplemental Table 4. Relative expression levels were calculated by the MyiQ system (Bio-Rad).

Titration of HTLV-1–specific antibodies

The titers of antibodies against HTLV-1 antigens in the plasma of infected mice were determined by the particle agglutination method using Serodia

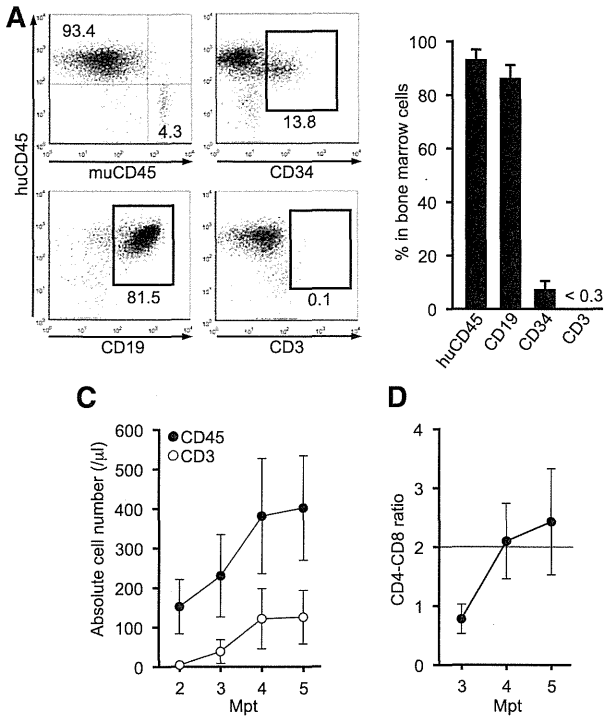

Figure 1. Generation of IBMI-huNOG mice and T-cell development in periphery. (A) Development of human leukocytes in bone marrow of IBMI-huNOG mice. Bone marrow cells from IBMI-huNOG mice (n = 20) at 1 mpt were analyzed by fluorescence-activated cell sorting (FACS) for expression of human CD45, CD19, and CD45, and mouse CD45 markers. Representatives (left) and the percentage of indicated markers (right) are shown. All cell populations were gated on mononuclear bone marrow cells. (B) Time course of human leukocyte development in the peripheral blood of IBMI-huNOG mice. Peripheral blood mononuclear cell (PBMC) from IBMI-huNOG mice (n = 40 for each time point) were stained for human CD45 at each time point. Box plots represent medians ± 1.5 IQR. (C) Increased number of human lymphocytes in IBMI-huNOG mice. Absolute numbers of human $CD45^+$ and $CD3^+$ cells in peripheral blood were determined by FACS analysis at each time point (n = 40 for each time point). (D) CD4-CD8 ratio in peripheral blood T cells. The CD4-CD8 ratio was calculated as follows: [(CD4 T-cell numbers per μL)/(CD8 T-cell numbers per μL)] (n = 40). (E) Sustained composition of human leukocytes in peripheral blood. PBMCs from IBMI-huNOG mice (n = 8) were stained for human CD45, CD3, and CD19. Results are presented as mean percentages of human $CD45^+$ cells.

HTLV-1 (Fuji Rebio).[23] To deplete human immunoglobulin M (IgM) or immunoglobulin G (IgG), streptavidin M-PVA magnetic beads (Chemagen) preincubated with biotin-conjugated goat anti–human IgM or IgG antibody (Sigma-Aldrich) were added to plasma from infected mice; a goat anti–mouse IgG antibody (Organon Teknika) was used as the negative control.

Bio-Plex cytokine assay

Plasma levels of IL-1b, IL-2, IL-4, IL-5, IL-6, IL-7, IL-8, IL-10, IL-12 (p70), IL-13, IL-17, granulocyte colony-stimulating factor (G-CSF), granulocyte macrophage colony-stimulating factor (GM-CSF), interferon-γ (IFN-γ), MCP-1, MIP-1β, and tumor necrosis factor α (TNF-α) in HTLV-1–infected and control mice were analyzed using the Bio-Plex Human Cytokine 17-Plex Panel (Bio-Rad) on a Bio-Plex 200 system according to the manufacturer's instructions.

Statistical analysis

The significance of differences was determined by Mann-Whitney *U* test, paired *t* test, or Spearman's rank-correlation coefficient (*r*); $P < .05$ was considered to indicate statistical significance.

Results

Reconstitution of human immune cells in NOG mice using IBMI

IBMI-huNOG mice were generated by IBMI of human $CD133^+$ hematopoietic stem cells into sublethally irradiated 6- to 7-week-old NOG mice. After 1 month of transplantation, human $CD45^+$ leukocytes were found to have almost completely reconstituted the bone marrow of recipient mice (Figure 1A). At this time point, the majority of the human leukocytes in bone marrow consisted of $CD19^+$ cells. A substantial number of $CD34^+$ cells were also detected, whereas human $CD3^+$ cells had not developed.

Less than half of peripheral blood cells were composed of human leukocytes even at 2 months posttransplantation (mpt). However, the number of human leukocytes increased in a time-dependent manner (Figure 1B-C). Between 3 and 4 mpt, the number of human $CD3^+$ T cells in the peripheral blood increased dramatically, as did the CD4-CD8 ratio (Figure 1D). $CD3^+$ T cells and the CD4-CD8 ratio reached stable levels by 4 to 5 mpt, suggesting that the development of human T cells was completed within this period.

Previous reports have shown that reconstituted human $CD45^+$ cells in other types of humanized mouse systems were overcome by $CD3^+$ T cells within several months of transplantation due to the reduction of B-cell development,[21,34] which may impair the integrity of host immunity. In contrast, the IBMI-huNOG mice model maintained a stable number of $CD3^+$ T cells as well as the B- to T-cell ratio in peripheral blood through at least 8 mpt (Figure 1E). Thus, the human immune system appeared to be effectively reconstituted in IBMI-huNOG mice, likely due to the enriched repopulation of long-term hematopoietic stem cells by direct injection of $CD133^+$ cells into the bone marrow cavity.[27]

Proliferation of HTLV-1–infected T cells in IBMI-huNOG mice

Human T lymphocytes fully developed in IBMI-huNOG mice within 4 to 5 mpt. These mice were then infected with HTLV-1 by intraperitoneal inoculation with 2.5×10^6 irradiated MT2 cells. The number of human $CD45^+$ leukocytes began to increase as early as 4 to 6 weeks postinoculation (wpi) and continued to increase rapidly thereafter (Figure 2A). HTLV-1 infection was also detected by 2 wpi, with the HTLV-1 PVL in peripheral blood increasing in a time-dependent manner (Figure 2B). The proportion of $CD3^+/CD45^+$ T lymphocytes was significantly enriched in HTLV-1–infected mice relative to mock-infected controls (Figure 2C), consistent with previous results.[16] Absence of residual MT2 cells used as the source of HTLV-1 was confirmed by MT2 cell-specific PCR as previously described (supplemental Figure 1).[35]

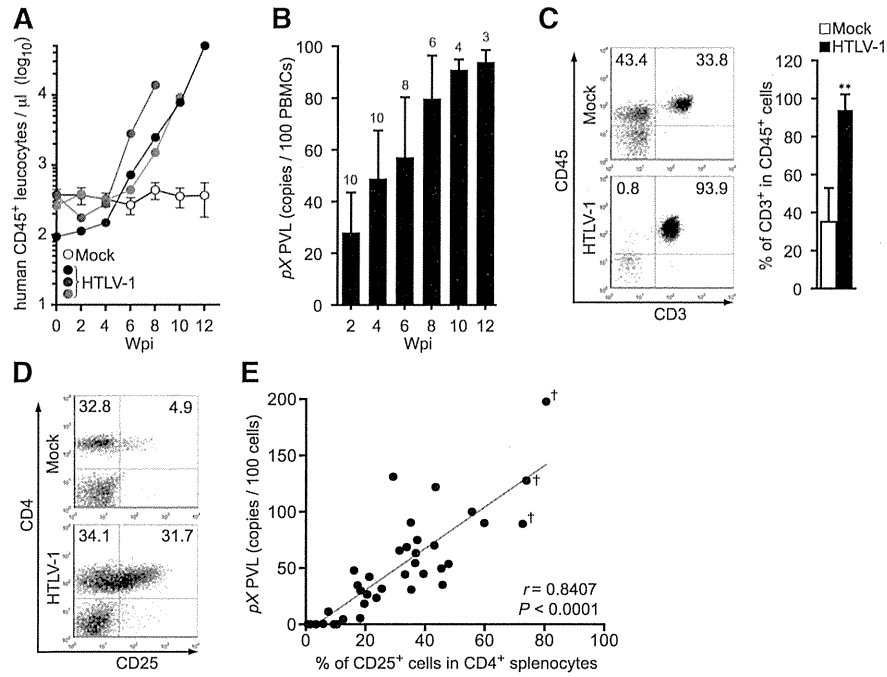

Figure 2. Kinetic analysis of HTLV-1 provirus in infected IBMI-huNOG mice. (A) Quantification of leukocyte numbers in the peripheral blood of HTLV-1–infected mice. Peripheral blood was routinely collected from mock- and HTLV-1–infected mice every 2 weeks. Human CD45$^+$ leukocytes were enumerated by FACS. Results from mock-infected mice (n = 10) are presented as mean ± standard deviation (SD), and representative results of 3 HTLV-1–infected mice are shown. (B) Quantification of HTLV-1 PVL in the peripheral blood of HTLV-1–infected mice. The PVL was determined by real-time PCR. Number at the top of each bar represents the number of analyzed HTLV-1–infected mice at each time point. (C) Expansion of CD3$^+$ T-cell populations in the peripheral blood of HTLV-1–infected mice. PBMCs from mock-infected (n = 3) and HTLV-1–infected mice (n = 18) were stained for human CD3 when sacrificed; the median value was 8 wpi. Results are presented as the average percentages ± SD of human CD45$^+$ cells. (D) Expansion of CD25$^+$ CD4 T cells in the spleen of HTLV-1–infected mice. Splenocytes were stained for human CD3, CD4, and CD25 and analyzed by FACS. Representative results from mock-infected (mouse ID: 8X20) and HTLV-1–infected (mouse ID: 8X01) mice are shown. (E) Correlation between the percentages of CD25$^+$ T cells and PVLs in the spleen. HTLV-1–infected mice (n = 37) were sacrificed to determine PVL and CD25$^+$ T-cell frequency in CD4$^+$ splenocytes. One dot represents the result of an individual HTLV-1–infected mouse. Spearman's rank-correlation coefficient (r) was adopted to identify statistically significant correlations between values. Daggers indicate that flower cells were observed in the peripheral blood of HTLV-1–infected mice.

HTLV-1–infected humanized mice showed marked expansion of CD25$^+$ CD4 T cells in the spleen relative to mock-infected controls (Figure 2D; Table 1), as is observed in peripheral blood of ATL and HAM/TSP patients.[9,36] Furthermore, PVLs in the spleen were significantly correlated with the rate of CD25$^+$ CD4 T cells (Figure 2E). These data suggest that the expanded CD25$^+$ CD4 T-cell population represents the majority of HTLV-1–infected cells in vivo.

ATL-like leukemic symptoms in HTLV-1–infected IBMI-huNOG mice

The majority of HTLV-1–infected mice exhibited splenomegaly, while apparent infiltration of infected T cells in the liver was observed in 3 infected mice with flower cells (Figure 3A; Table 1) and the weight of liver in these mice was remarkably increased (HTLV-1: 1550 ± 620 mg [n = 3]; mock: 715 ± 85 mg [n = 3]). When PVLs of several lymphoid organs were analyzed, the proportions of infected cells in the bone marrow and lymph nodes were significantly lower than those in the spleen and peripheral blood, consistent with the leukemic phenotype of infected mice (Figure 3B). This result is in striking contrast to other humanized mouse models, in which HTLV-1 infection[17] or the ectopic expression of Tax[16] preferentially induce lymphoma.

May-Grunwald Giemsa staining of peripheral blood smears from infected mice revealed the presence of large, abnormal leukemic cells with lobulated nuclei, which were morphologically identical to the flower cells observed in ATL patients (Figure 3D-E).[8] The activated phenotype of infected T cells was also evident, with clear downregulation of CD3 expression on the surface of peripheral T cells in HTLV-1–infected mice, similar to that seen in ATL cells (Figure 3C).[37]

ATL cells have been shown to secrete proinflammatory cytokines, such as IL-6, TNF-α, and GM-CSF, which stimulate activation and proliferation of infected T cells and promote development of ATL leukemogenesis.[38-40] Analysis of cytokine and chemokine levels in the plasma of HTLV-1–infected mice revealed significantly elevated levels of several proinflammatory cytokines (Figure 4). The concentration of IFNγ significantly correlated with PVL in the peripheral blood (supplemental Figure 2), suggesting Th1 immune responses induced in infected mice. Together, these results suggest that HTLV-1–infected IBMI-huNOG mice accurately recreate many of the pathological features of ATL, including hepatosplenomegaly, leukemic T-cell overgrowth with lobulated nuclei, hypercytokinemia, and downregulation of CD3 on T cells.

Oligoclonal proliferation of human T-cell clones in HTLV-1–infected IBMI-huNOG mice

To evaluate the clonal proliferation of HTLV-1–infected T cells in infected mice, we quantified cellular clonality using clone-specific real-time PCR analysis. Splenocytes were isolated from 8 infected mice sacrificed at various time points, and genomic DNA fragments

Table 1. Pathological features of mock- or HTLV-1–infected IBMI-huNOG mice

Mouse ID*	Wpi†	PVL‡	$CD3^+CD4^+$ (%)§	$CD4^+CD25^+$ (%)§	Spleen weight (mg)	Lymph node weight (mg)‖	Observations
8807	—	—	16.7	2.6	45	1	Mock infected
8X10	—	—	20.2	3.4	51	3	Mock infected
8X20	—	—	36.5	4.4	40	2	Mock infected
8401	17	65.6	53.1	31.4	195	23	
8402	11	0.1	5.3	0.7	26	1	
8403	14	0.1	10.8	3.4	35	1	
8404	17	5.4	53.4	18.3	68	2	
8405	12	11.3	30.3	7.6	59	14	
8406	5	0.1	10.5	1.5	33	3	
8407	8	4.5	69.6	12.5	166	9	
8801	25	0.1	59.6	10.4	187	7	
8803	30	0.4	38.6	5.8	55	11	
8804	23	0.1	46.6	9.5	105	5	
8805	8	70.0	57.0	43.1	233	37	Leukemia
8808	8	26.5	52.5	20.6	101	40	
8810	4	42.2	55.4	21.3	40	22	
8X01	5	44.9	65.8	39.5	208	11	
8X04	8	121.9	62.2	43.5	165	7	Leukemia
8X05	23	127.7	81.4	73.9	226	8	Leukemia, flower cells (10.6%),¶ tumor lesion
8X06	9	31.6	50.5	25.5	155	5	
8X09	5	34.6	52.2	17.4	227	9	
8X12	4	47.9	58.5	16.2	188	11	
8X14	25	68.6	51.4	33.8	145	25	Leukemia
8X16	7	90.4	78.9	35.2	200	16	Leukemia
8X17#	9	131.1	44.6	29.3	200	35	Leukemia
8X18	18	197.7	89.4	80.5	358	28	Leukemia, flower cells (19.2%),¶ tumor lesion
9Z01	10	53.6	75.8	47.9	220	12	Leukemia
9Z03	6	23.4	51.6	23.7	38	18	
9Z17	6	18.2	64.7	19.7	163	10	
9Z18	16	89.2	80.4	72.7	285	5	Leukemia, flower cells (4.2%),¶ tumor lesion
9Z19	6	35.0	65.0	45.9	207	20	
X202	12	90.0	76.6	59.9	353	13	Leukemia
X206	8	54.4	56.6	36.7	317	15	
X207**	11	100.0	62.2	55.7	358	6	Leukemia
X208	4	29.9	74.7	18.4	188	15	
X209	7	30.8	74.4	35.4	270	21	
X212	9	74.9	56.8	37.4	270	5	Leukemia
X214	10	44.3	48.0	33.3	170	6	
X216	8	63.2	66.1	36.9	271	12	Leukemia
X217	7	49.6	76.9	45.5	306	18	Leukemia

Leukemia, infected mice with atypical lymphocytes >90% of PBMCs; flower cells, atypical lymphocytes with >4 lobulated nuclei in a cell; tumor lesion, tumor formation of infiltrating infected T cells in the liver.

*The 37 infected mice listed are identical to those in Figure 2E.

†The wpi when indicated mice were sacrificed.

‡PVL is expressed as number of *pX* copies per 100 cells.

§The population of indicated marker-positive cells in $CD45^+$ splenocytes.

‖The weight value of one of the largest mesenteric lymph node in each mouse.

¶The percentage of flower cells in total lymphocytes in blood smear (presented in parentheses).

#High proportion of $CD25^+$ CD8 T cells in PBMCs.

**High proportion of DP T cells in PBMCs.

flanking the major integration sites in the HTLV-1–infected cells were amplified by IL-PCR. Amplified DNA fragments were subcloned into plasmids and sequenced to confirm proper integration (supplemental Table 5). As shown in Figure 5A, the occupancy of detected clones determined by real-time PCR was < 5% in cells harvested 5 to 8 wpi, indicating polyclonal HTLV-1 infection in these mice. In contrast, 2 mice sacrificed after prolonged infection periods (18 and 23 wpi, respectively) produced high percentages of infected clones. Interestingly, these 2 mice also showed overgrowth of $CD25^+$ CD4 T cells with flower-shaped nuclei, characteristic of ATL cells (Figure 3D-E), whereas such cells were not observed in the 6 remaining mice. These findings indicate that a limited number of HTLV-1–infected T-cell clones selectively proliferated in the spleens of infected mice, resulting in an ATL-like leukemic phenotype.[33,41]

Presence of identical infected clones in $CD25^-$ and $CD25^+$ CD4 T-cell populations

Splenocytes from infected mice were sorted into $CD25^-$ or $CD25^+$ CD4 T cells and CD8 T cells; the PVL of each population was also determined. Most of the $CD25^+$ CD4 T cells isolated from the spleens of infected mice were provirus-positive, as was a significant proportion of $CD25^-$ CD4 T cells, whereas infection of CD8 T cells was rare (Figure 5B). Interestingly, *tax* expression in HTLV-1–infected $CD25^+$ CD4 T cells was suppressed compared with that in

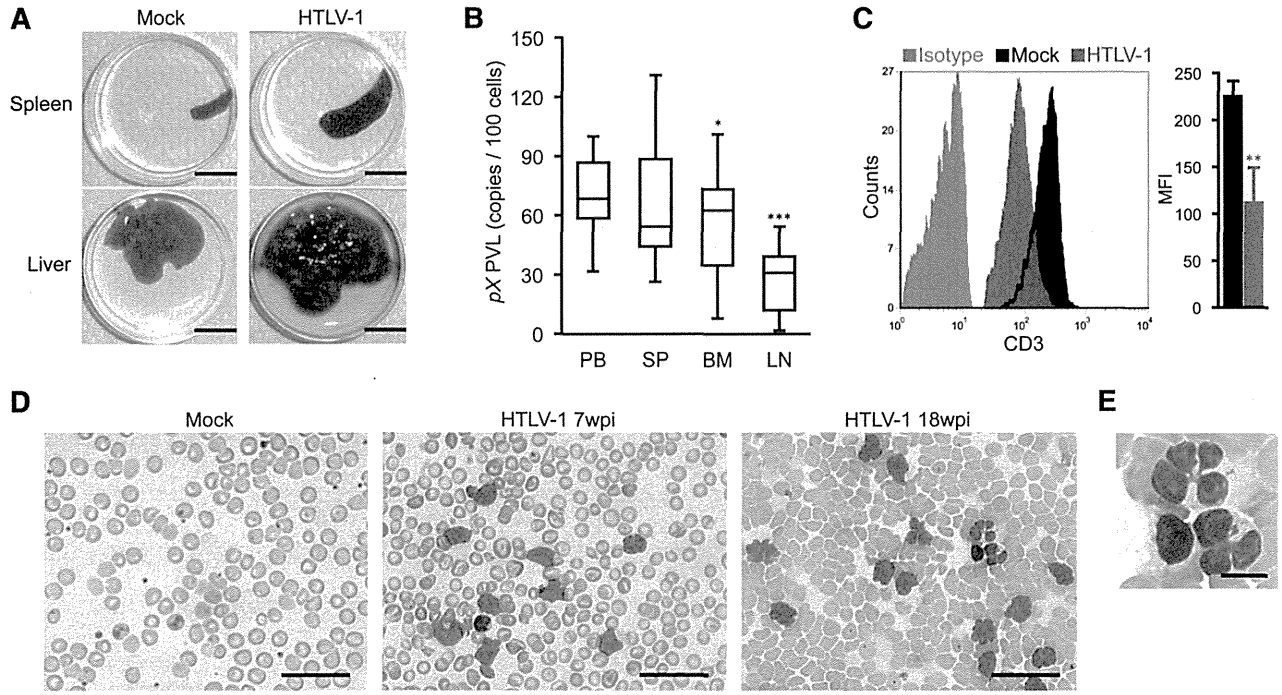

Figure 3. Splenomegaly and leukemic T-cell overgrowth in infected IBMI-huNOG mice. (A) Hepatosplenomegaly in HTLV-1–infected mice. Representative spleens and livers from mock- and HTLV-1–infected mice are shown. Scale bars in panel A represent 10 mm. (B) PVL in lymphoid organs of HTLV-1–infected mice. PVL in the peripheral blood (PB), spleen (SP), bone marrow (BM), and lymph nodes (LM) of HTLV-1–infected mice (n = 17) are shown. Box plots represent medians ± 1.5 IQR. Asterisks indicate statistical significance vs the value obtained from peripheral blood (*$P < .05$, ***$P < .001$ by paired *t* test). (C) Downregulation of CD3 on the T-cell surface. PBMCs from mock- (n = 3) and HTLV-1–infected mice (n = 18) were stained for human CD3 and analyzed by FACS. Results are presented as mean MFI ± SD of CD3 expression. (D-E) Smears of peripheral blood from HTLV-1–infected mice showing a number of leukemic cells with atypically shaped nuclei. Results from two infected mice (7 and 18 wpi, respectively) and a mock-infected mouse (at 8 mpt) are shown. Higher-magnification view of flower cells in panel D is shown in panel E. Scale bars in panels D-E represent 50 and 10 μm, respectively. Asterisks in panels B and C represent significant differences vs mock-infected mice (**$P < .01$ by Mann-Whitney *U* test).

$CD25^-$ CD4 T cells; however, higher *HBZ* expression was observed in $CD25^+$ CD4 T cells (Figure 5C).

Further clonality analysis for HTLV-1–infected $CD25^-$ and $CD25^+$ CD4 T cells isolated from the same spleen with the purity of >95% (supplemental Figure 3) revealed that the most abundant clone was the same in both T-cell populations; however, the occupancy was higher in the $CD25^+$ population (Figure 5D), indicating the preferential growth of infected clones with CD25 expression.

Induction of HTLV-1–specific adaptive immune responses in HTLV-1–infected IBMI-huNOG mice

HLA-A*24:02–restricted Tax-specific CTLs were frequently detected in ATL patients, and are known to play an important role in the control of HTLV-1–infected cells in vivo.[42-44] To investigate whether Tax-specific CTLs were induced in HTLV-1–infected mice, the IBMI-huNOG mice were generated using hematopoietic stem cells purified from the cord blood of an HLA-A*24:02 haplotype individual. HLA-A*24:02 tetramers coupled with Tax301-309 were used to detect CTLs. The cord blood HLA-A alleles used in this study are shown in supplemental Table 1. As shown in Figure 6A, Tax301-309–specific CTLs were detected in HTLV-1–infected mice at a frequency similar to that of ATL patients (0.7% ± 0.8%, n = 18),[45] whereas control tetramer CTLs specific for HIV env produced only marginal staining of CD8 T cells.

To evaluate whether functionally reactive Tax301-309–specific CTLs were present in infected mice, we cultured splenocytes from HTLV-1–infected mice in the presence of Tax peptide. Tax301-309 specific CTLs clearly proliferated following peptide stimulation; no reaction was seen in controls. Furthermore, the frequency of Tax301-309–specific CTLs in in vivo CD8 T cells was inversely correlated with the PVLs of HTLV-1–infected mice (Figure 6B). These results suggest that HTLV-1–infected mice induce functional T-cell–mediated cellular immunity against HTLV-1, which may be involved in the control of HTLV-1–infected cells in vivo.

Antibodies against HTLV-1 antigens were also detected in the plasma of infected mice as early as 2 wpi, whereas the specific antibody was not detected before infection (Figure 6C). The titer of HTLV-1–specific antibodies increased in all cases until 4 wpi, followed by a gradual decline in 67% of infected mice (4 of 6), coincident with a decrease in body weight. However, 2 of the infected mice exhibited a reactivation of antibody production at 8 wpi, suggestive of immunoglobulin class switching from IgM to IgG. In fact, HTLV-1–specific antibody titers were significantly decreased following selective depletion of human IgG, indicating the presence of functional IgG in the plasma of HTLV-1–infected mice (Figure 6D). These data clearly support the notion that the functional interaction between human T and B cells required for class switching exists in this model. Taken together, these results demonstrate that human-like adaptive immunity against HTLV-1 was established in the HTLV-1–infected IBMI-huNOG mice.

Discussion

In this study, we established a novel humanized mouse model of HTLV-1 infection. To generate humanized mice, we transplanted

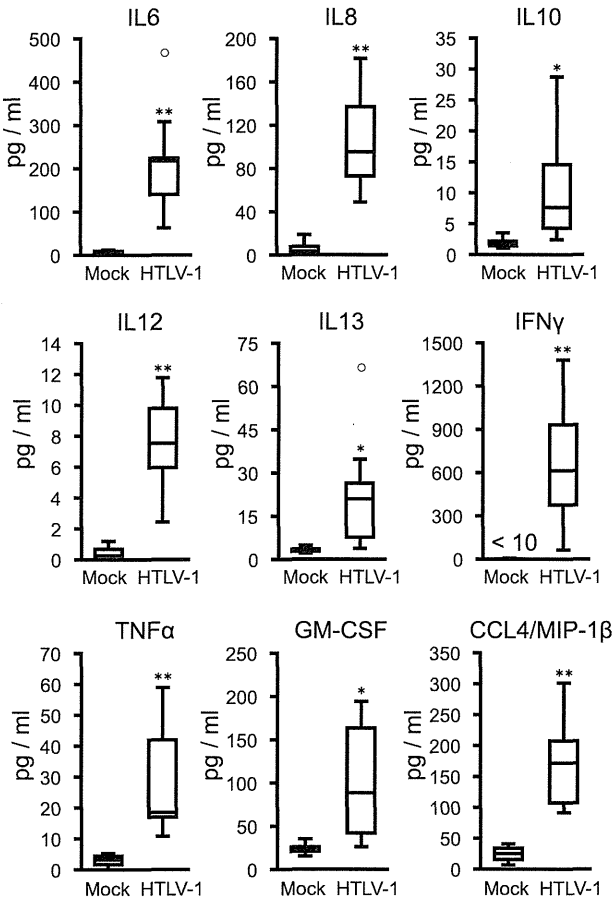

Figure 4. Induction of inflammatory cytokines in infected IBMI-huNOG mice. Human cytokine concentrations in plasma. Plasma was collected following sacrifice of mock-infected (n = 4) and HTLV-1–infected mice (n = 8). Seventeen cytokines were quantified using a cytokine bead array system. The concentrations of human IL-6, IL-8, IL-10, IL-12, IL-13, IFNγ, TNF-α, GM-CSF, and CCL4/MIP-1β are shown, all of which were significantly increased in the plasma of HTLV-1–infected mice. Increased expressions of the other 6 cytokines (IL-2, IL-4, IL-7, IL-17, G-CSF, and MCP-1) were also observed in infected mice but not statistically significant. On the other hand, little decrease in the concentrations of IL-1 and IL-5 was seen. Asterisks in each panel represent significant differences vs mock-infected mice (*$P < .05$, **$P < .01$ by Mann-Whitney U test).

human stem cells directly into the bone marrow cavity of NOD/Shi-SCID/IL-2Rγc null (NOG) mice using an IBMI method.

The efficacy of humanization achieved in this model is markedly superior to other procedures, such as intrahepatic or intravenous injection of human hematopoietic stem cells.[21,22,29] While T-lineage–cell populations become dominant over B-cell populations in the lymphoid organs of other humanized mouse systems within a few months after transplantation, in IBMI-huNOG mice the B-to-T-cell ratio remained constant for >8 months posttransplantation (Figure 1E). One possible explanation for this difference is that direct injection of hematopoietic stem cell preparations into the bone marrow of recipient mice improves the colonization efficiency of long-term stem cells.[27,46] Moreover, we used $CD133^+$ cells to generate IBMI-huNOG mice. CD133, the early hematopoietic progenitor cell marker, is thought to be ancestral to CD34 in human hematopoiesis.[47] Previous studies have revealed that $CD133^+$ cells were capable of differentiating not only into hematopoietic cells but also into endothelial, stromal, neuronal, and other type of cells.[47-49] It is possible that human mesenchymal stromal cells derived from $CD133^+$ cells support the development and maintenance of human B cells in the bone marrow microenvironment.

Having established a new humanized mouse model, we then infected IBMI-huNOG mice with HTLV-1 through inoculation with sublethally irradiated HTLV-1–producing cells.[28] HTLV-1–infected IBMI-huNOG mice recapitulated a large number of pathological features characteristic of ATL patients, including hyperproliferation of $CD3^+$ T cells, clonal proliferation of $CD25^+$ CD4 T cells, the appearance of flower cells in the periphery, hepatosplenomegaly, inflammatory hypercytokinemia, and down-regulation of CD3 on T cells.

Overgrowth of infected T cells was correlated with the expression of CD25 on CD4 T cells, consistent with recent reports.[17] However, the substantial proportion of $CD25^-$ CD4 T cells were also infected and identical T-cell clones, as determined by provirus integration site, were detected as the most abundant clones in both $CD25^-$ and $CD25^+$ CD4 T-cell populations, suggesting that CD25 expression likely occurs after infection in the course of clonal expansion. In addition, the expressions of *tax* and CD25 were inversely correlated. Further research will be necessary to identify molecular events associated with the suppression of *tax* expression in HTLV-1–infected $CD25^+$ CD4 T cells in relation to the development of ATL.

Banerjee et al[16] described the development of T-cell lymphoma following bone marrow transplantation of HTLV-1–infected $CD34^+/CD38^-$ hematopoietic stem cells into a NOD/SCID mouse. The lymphoma cells in these mice were capable of infiltrating into multiple organs but represented only $CD25^-$ or $CD25^{low}$ phenotypes. In contrast, HTLV-1–infected IBMI-huNOG mice developed leukemia in $CD25^+$ CD4 T cells, similar to that observed in ATL patients. The mechanism underlying this difference is unknown but may be due to differences in the developmental stage of T cells at the time of infection. Indeed, HTLV-1 infection in a different humanized mouse model, generated by intrahepatic transplantation of human $CD34^+$ stem cells into $Rag2^{-/-}\gamma c^{-/-}$ mice, induced formation of thymomas/lymphomas in mature CD4 T cells.[17] In this case, HTLV-1 infection was carried out 4 and 8 weeks after transplantation of $CD34^+$ hematopoietic stem cells, giving the human immune system time to develop. Thus the infection of $CD34^+$ stem cells per se does not appear to be sufficient for the induction of mature $CD25^+$ T cell malignancies and may require more developed lymphoid cells or a more appropriate microenvironment capable of supporting cell development.

Furthermore, HTLV-1–infected IBMI-huNOG mice almost exclusively developed leukemia, whereas HTLV-1 infection in the other humanized mouse models described above preferentially induced formation of lymphoma or thymoma. The reason for this difference is not clear but may stem from differences in the timing of T-cell infection. IBMI-huNOG mice were infected after the human hematopoietic system had been fully established, while in the other systems the infection was carried out before or shortly after stem cell transplantation.

In addition to leukemic growth of $CD25^+$ T cells, we also observed formation of flower cells in the peripheral blood of infected mice at later time points postinfection (>16 wpi). Although transformed T cells derived from Tax-transgenic mice were found to exhibit similar morphology,[15] none of the animal models described so far had recapitulated this pathology. Clonal analysis performed as part of this study demonstrated that the expansion of $CD25^+$ T-cell clones preceded the appearance of flower cells in periphery, suggesting a sequence of events that occurs during development of the malignancy. Thus, chronological

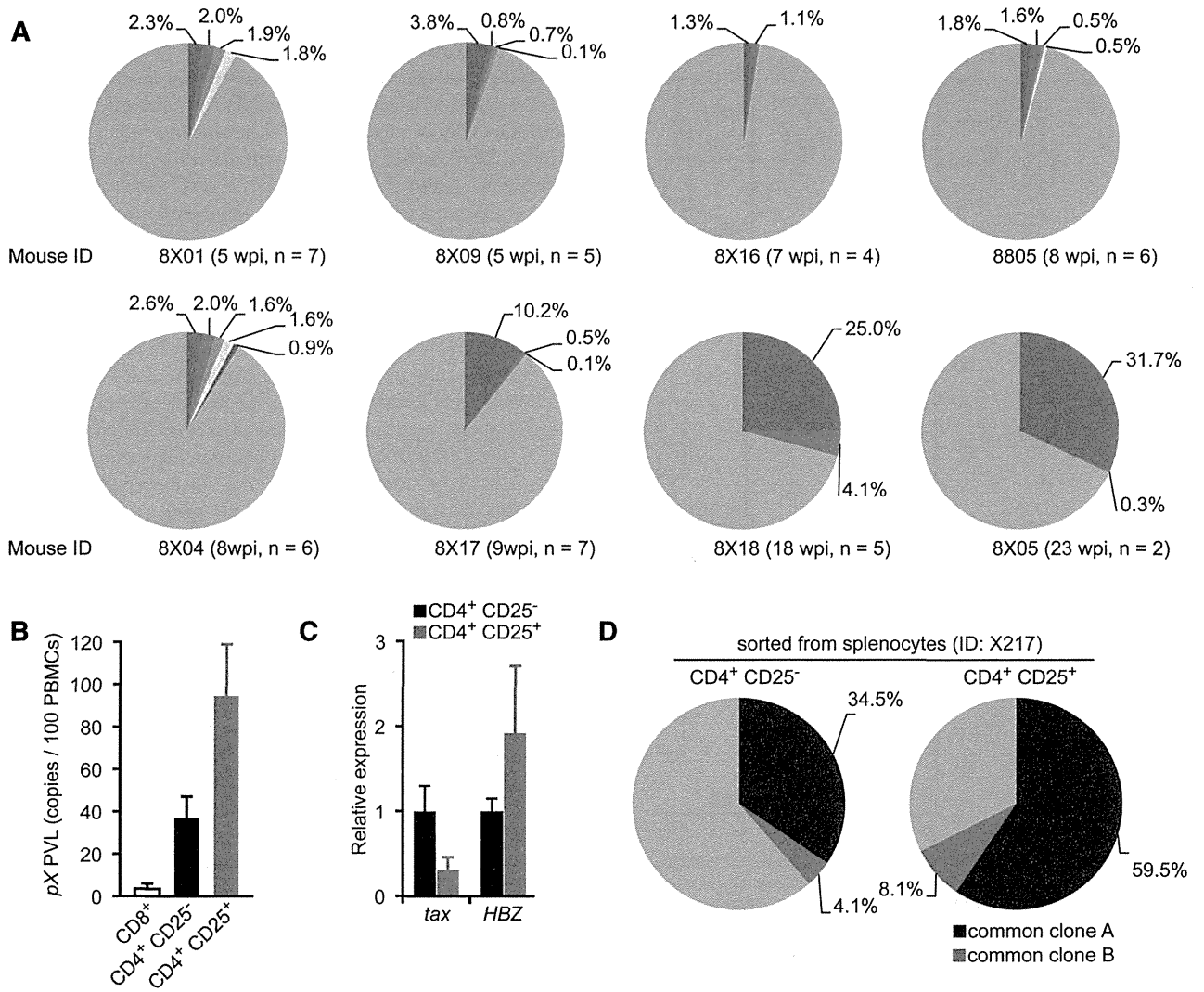

Figure 5. Progression of clonality in splenocytes of infected IBMI-huNOG. (A) Occupancy of HTLV-1–infected clones in the spleen. Abundant integration sites of HTLV-1 provirus were amplified by IL-PCR and subcloned into plasmids. The number of integration sites in each splenic DNA sample was determined by quantitative PCR using the clone-specific nucleotide sequence for each integration site. Results from 8 individual HTLV-1–infected mice are shown as pie charts. Size of the slice is proportional to the relative abundance of T-cell clones successfully amplified by IL-PCR, while data of minor clones with less than 0.1% occupancy were omitted. Gray regions represent clones with undefined integration sites. n, number of integration sites determined by nucleotide sequence of cloned PCR fragments in each mouse. (B) PVLs of specifiedT-cell populations. Splenocytes from HTLV-1–infected mice (n = 5) were sorted into $CD25^-$ or $CD25^+$ CD4 T cells and $CD8^+$ T cells. Genomic DNA isolated from each T-cell population was analyzed for PVL by real-time PCR using primers for the *pX* region of HTLV-1. (C) Comparative analysis of viral transcripts in $CD25^-$ and $CD25^+$ CD4 T-cell populations. Splenocytes from HTLV-1–infected mice (n = 5) are identical to those in mentioned above. The expression levels of *tax* (left) and *HBZ* (right) were analyzed by quantitative RT-PCR and were normalized to that of *HPRT1*. Results are presented as the fold change compared with the value in $CD25^-$ CD4 T cells. (D) Detection of common T-cell clones in the $CD25^-$ and $CD25^+$ CD4 T-cell populations. Clonal occupancy in both $CD25^-$ and $CD25^+$ populations are presented as pie charts. Two abundant common clones were analyzed for occupancy. Identified integration sites are listed in supplemental Table 5. The purity of each sorted population was >95% (supplemental Figure 3).

analysis of genetic and/or biochemical events in infected T cells from this mouse model should provide substantial information regarding the development of ATL.

We detected HLA-restricted CTLs against Tax protein of HTLV-1, as demonstrated in the peripheral blood of HTLV-1–infected carriers,[43] confirming the presence of an acquired immune response. Furthermore, the frequency of CTLs in CD8 T-cell populations were inversely correlated with the number of infected T cells in the spleen of humanized mice, similar to observations in HTLV-1–infected individuals.[43] The presence of functional T cells was also supported by the production of IgG antibodies specific to HTLV-1. Although humanized mice established by the transplantation of $CD34^+$ hematopoietic stem cells have been reported to produce antibodies against specific pathogens such as EBV,[22] HIV-1,[21] and DENV,[50] class switching from IgM to IgG was observed in only a few cases, likely due to immature T-cell development. In the IBMI-huNOG system, however, IgG production against HTLV-1 structural protein was observed after biphasic induction of antibodies after 8 weeks, indicating a functional interaction between CD4 T cells and B cells specific for viral antigens. Taken together, these data demonstrate induction of an adaptive immune response against HTLV-1 in HTLV-1–infected IBMI-huNOG mice, which may play an important role as selective pressure in the expansion of malignant T-cell clones.

In conclusion, our study demonstrates that the HTLV-1–infected IBMI-huNOG mouse represents a novel model that will facilitate elucidation of the molecular mechanism of in vivo development of ATL. Moreover, our model can also be used to develop and evaluate

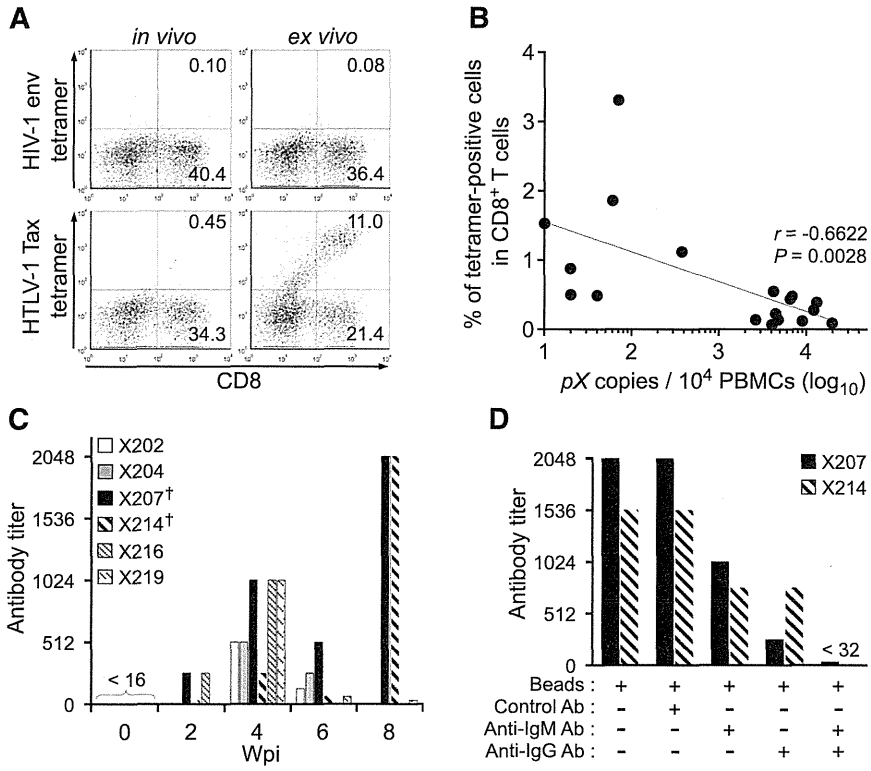

Figure 6. Induction of cellular and humoral immune responses against HTLV-1 in infected IBMI-huNOG mice. (A) Detection of HTLV-1–specific HLA-A*24:02-restricted CTLs. Splenocytes from HTLV-1–infected mice at 8 wpi were stained with human CD8 and Tax301-309 tetramer or HIV-1 env gp160 tetramer as a negative control, respectively. Representative results of tetramer-positive CD8 T cells in vivo (left) and ex vivo culture with Tax peptide (right) are shown. (B) Inverse correlation between PVL and the frequency of Tax301-309–specific CTLs. The percentages of tetramer-positive CD8 T cells and PVL in the spleens of 18 HTLV-1–infected mice are shown. One dot represents the result of an individual HTLV-1–infected mouse. Spearman's rank-correlation coefficient (r^2) was used to identify statistically significant correlations. (C) HTLV-1–specific antibody responses in HTLV-1–infected mice. HTLV-1–specific antibody titers in plasma were monitored by the particle agglutination method. Each bar represents an individual mouse. The plasma of indicated mice prior to infection were used as negative-controls (shown as 0 wpi), and these titers were undetectable level (<16). Mice with daggers (mouse ID: X207 and X214) showed biphasic induction of antibody responses; titers peaked at 8 wpi. (D) Detection of HTLV-1–specific IgM or IgG antibody. Antibody depletion was performed by addition of goat antibodies against human IgG or IgM and anti-goat antibody conjugated magnetic beads to the plasma of two mice, as shown in panel C (indicated by daggers). Bars represent antibody titers in the individual X207 and X214 mice. Ab, antibody.

novel preclinical therapies that target viral gene products or cellular molecules critical for viral replication as well as evaluate the efficacy of vaccine candidates to prevent viral expansion in vivo.

Acknowledgments

The authors thank Drs R. Tatsumi and Y. Adachi for advice in establishing humanized mice and assistance with the pathological analysis, respectively. The authors are grateful to the Japanese Red Cross Kinki Cord Blood Bank for providing the samples used in this study.

This work was supported by Grants-in-Aid for Scientific Research C from the Ministry of Education, Culture, Sports, Science and Technology of Japan (grants 21590515 and 24590562) (J.F.); a MEXT-Supported Program for the Strategic Research Foundation at Private Universities; and Health and Labour Sciences Research Grants for Research on Emerging and Re-emerging Infectious Diseases from Ministry of Health, Labour and Welfare (grant 24171601) (T.U.) (grant 23211801) (M. Tanaka).

Authorship

Contribution: K.T. and J.F. designed the research; K.T. and R.X. established and maintained humanized mice; K.T., R.X., M. Tei and T.U. carried out experiments; M. Tanaka was involved in the IL-PCR analysis; K.T., R.X., M. Tei, and J.F. analyzed results; N.T. performed statistical analysis; K.T. designed the figures; and K.T. and J.F. wrote the paper.

Conflict-of-interest disclosure: The authors declare no competing financial interests.

Correspondence: Jun-ichi Fujisawa, Department of Microbiology, Kansai Medical University, 2-5-1 Shin-machi, Hirakata, Osaka 573-1010, Japan; e-mail: fujisawa@hirakata.kmu.ac.jp.

References

1. Hinuma Y, Nagata K, Hanaoka M, et al. Adult T-cell leukemia: antigen in an ATL cell line and detection of antibodies to the antigen in human sera. *Proc Natl Acad Sci USA.* 1981;78(10):6476-6480.
2. Poiesz BJ, Ruscetti FW, Gazdar AF, Bunn PA, Minna JD, Gallo RC. Detection and isolation of type C retrovirus particles from fresh and cultured lymphocytes of a patient with cutaneous T-cell lymphoma. *Proc Natl Acad Sci USA.* 1980;77(12):7415-7419.
3. Osame M, Usuku K, Izumo S, et al. HTLV-I associated myelopathy, a new clinical entity. *Lancet.* 1986;1(8488):1031-1032.
4. Kondo T, Kono H, Miyamoto N, et al. Age- and sex-specific cumulative rate and risk of ATLL for HTLV-I carriers. *Int J Cancer.* 1989;43(6):1061-1064.
5. Boxus M, Twizere JC, Legros S, Dewulf JF, Kettmann R, Willems L. The HTLV-1 Tax interactome. *Retrovirology.* 2008;5:76.
6. Matsuoka M, Jeang KT. Human T-cell leukemia virus type 1 (HTLV-1) and leukemic transformation: viral infectivity, Tax, HBZ and therapy. *Oncogene.* 2011;30(12):1379-1389.
7. Yoshida M, Seiki M, Yamaguchi K, Takatsuki K. Monoclonal integration of human T-cell leukemia provirus in all primary tumors of adult T-cell leukemia suggests causative role of human T-cell leukemia virus in the disease. *Proc Natl Acad Sci USA.* 1984;81(8):2534-2537.
8. Shimoyama M, Minato K, Tobinai K, et al. Atypical adult T-cell leukemia-lymphoma: diverse clinical manifestations of adult T-cell leukemia-lymphoma. *Jpn J Clin Oncol.* 1983;13(Suppl 2):165-187.
9. Okayama A, Tachibana N, Ishihara S, et al. Increased expression of interleukin-2 receptor alpha on peripheral blood mononuclear cells in HTLV-I tax/rex mRNA-positive asymptomatic carriers. *J Acquir Immune Defic Syndr Hum Retrovirol.* 1997;15(1):70-75.

10. Bieberich CJ, King CM, Tinkle BT, Jay G. A transgenic model of transactivation by the Tax protein of HTLV-I. *Virology.* 1993;196(1):309-318.
11. Feuer G, Zack JA, Harrington WJ Jr, et al. Establishment of human T-cell leukemia virus type I T-cell lymphomas in severe combined immunodeficient mice. *Blood.* 1993;82(3): 722-731.
12. Kondo A, Imada K, Hattori T, et al. A model of in vivo cell proliferation of adult T-cell leukemia. *Blood.* 1993;82(8):2501-2509.
13. Furuta RA, Sugiura K, Kawakita S, Inada T, Ikehara S, Matsuda T, Fujisawa J. Mouse model for the equilibration interaction between the host immune system and human T-cell leukemia virus type 1 gene expression. *J Virol.* 2002;76(6): 2703-2713.
14. Dewan MZ, Terashima K, Taruishi M, et al. Rapid tumor formation of human T-cell leukemia virus type 1-infected cell lines in novel NOD-SCID/ gammac(null) mice: suppression by an inhibitor against NF-kappaB. *J Virol.* 2003;77(9): 5286-5294.
15. Hasegawa H, Sawa H, Lewis MJ, et al. Thymus-derived leukemia-lymphoma in mice transgenic for the Tax gene of human T-lymphotropic virus type I. *Nat Med.* 2006;12(4):466-472.
16. Banerjee P, Tripp A, Lairmore MD, et al. Adult T-cell leukemia/lymphoma development in HTLV-1-infected humanized SCID mice. *Blood.* 2010;115(13):2640-2648.
17. Villaudy J, Wencker M, Gadot N, et al. HTLV-1 propels thymic human T cell development in "human immune system" Rag2$^{-/-}$ gamma c$^{-/-}$ mice. *PLoS Pathog.* 2011;7(9):e1002231.
18. Satou Y, Yasunaga J, Zhao T, et al. HTLV-1 bZIP factor induces T-cell lymphoma and systemic inflammation in vivo. *PLoS Pathog.* 2011;7(2): e1001274.
19. Kazanji M. HTLV type 1 infection in squirrel monkeys (Saimiri sciureus): a promising animal model for HTLV type 1 human infection. *AIDS Res Hum Retroviruses.* 2000;16(16):1741-1746.
20. Lairmore MD, Silverman L, Ratner L. Animal models for human T-lymphotropic virus type 1 (HTLV-1) infection and transformation. *Oncogene.* 2005;24(39):6005-6015.
21. Watanabe S, Terashima K, Ohta S, et al. Hematopoietic stem cell-engrafted NOD/SCID/ IL2Rgamma null mice develop human lymphoid systems and induce long-lasting HIV-1 infection with specific humoral immune responses. *Blood.* 2007;109(1):212-218.
22. Yajima M, Imadome K, Nakagawa A, et al. A new humanized mouse model of Epstein-Barr virus infection that reproduces persistent infection, lymphoproliferative disorder, and cell-mediated and humoral immune responses. *J Infect Dis.* 2008;198(5):673-682.
23. Hasegawa A, Ohashi T, Hanabuchi S, Kato H, Takemura F, Masuda T, Kannagi M. Expansion of human T-cell leukemia virus type 1 (HTLV-1) reservoir in orally infected rats: inverse correlation with HTLV-1-specific cellular immune response. *J Virol.* 2003;77(5):2956-2963.
24. Kannagi M, Hasegawa A, Kinpara S, Shimizu Y, Takamori A, Utsunomiya A. Double control systems for human T-cell leukemia virus type 1 by innate and acquired immunity. *Cancer Sci.* 2011; 102(4):670-676.
25. Ito M, Hiramatsu H, Kobayashi K, et al. NOD/SCID/gamma(c)(null) mouse: an excellent recipient mouse model for engraftment of human cells. *Blood.* 2002;100(9):3175-3182.
26. Kushida T, Inaba M, Hisha H, et al. Intra-bone marrow injection of allogeneic bone marrow cells: a powerful new strategy for treatment of intractable autoimmune diseases in MRL/lpr mice. *Blood.* 2001;97(10):3292-3299.
27. Wang J, Kimura T, Asada R, et al. SCID-repopulating cell activity of human cord blood-derived CD34- cells assured by intra-bone marrow injection. *Blood.* 2003;101(8):2924-2931.
28. Miyoshi I, Kubonishi I, Yoshimoto S, et al. Type C virus particles in a cord T-cell line derived by co-cultivating normal human cord leukocytes and human leukaemic T cells. *Nature.* 1981; 294(5843):770-771.
29. Nie C, Sato K, Misawa N, et al. Selective infection of CD4+ effector memory T lymphocytes leads to preferential depletion of memory T lymphocytes in R5 HIV-1-infected humanized NOD/SCID/IL-2Rgammanull mice. *Virology.* 2009;394(1):64-72.
30. Takamori A, Hasegawa A, Utsunomiya A, et al. Functional impairment of Tax-specific but not cytomegalovirus-specific CD8+ T lymphocytes in a minor population of asymptomatic human T-cell leukemia virus type 1-carriers. *Retrovirology.* 2011;8:100.
31. Ueno S, Umeki K, Takajo I, et al. Proviral loads of human T-lymphotropic virus Type 1 in asymptomatic carriers with different infection routes. *Int J Cancer.* 2012;130(10):2318-2326.
32. Etoh K, Tamiya S, Yamaguchi K, et al. Persistent clonal proliferation of human T-lymphotropic virus type I-infected cells in vivo. *Cancer Res.* 1997; 57(21):4862-4867.
33. Umeki K, Hisada M, Maloney EM, Hanchard B, Okayama A. Proviral loads and clonal expansion of HTLV-1-infected cells following vertical transmission: a 10-year follow-up of children in Jamaica. *Intervirology.* 2009;52(3):115-122.
34. Hiramatsu H, Nishikomori R, Heike T, Ito M, Kobayashi K, Katamura K, Nakahata T. Complete reconstitution of human lymphocytes from cord blood CD34+ cells using the NOD/SCID/ gammacnull mice model. *Blood.* 2003;102(3): 873-880.
35. Nitta T, Tanaka M, Sun B, Hanai S, Miwa M. The genetic background as a determinant of human T-cell leukemia virus type 1 proviral load. *Biochem Biophys Res Commun.* 2003;309(1):161-165.
36. Yamano Y, Araya N, Sato T, et al. Abnormally high levels of virus-infected IFN-gamma+ CCR4+ CD4+ CD25+ T cells in a retrovirus-associated neuroinflammatory disorder. *PLoS ONE.* 2009;4(8):e6517.
37. Matsuda M, Maeda Y, Shirakawa C, et al. CD3 down-regulating factor in sera and culture supernatants of leukaemic cells from patients with adult T cell leukaemia. *Br J Haematol.* 1993;83(2): 212-217.
38. Yamada Y, Ohmoto Y, Hata T, et al. Features of the cytokines secreted by adult T cell leukemia (ATL) cells. *Leuk Lymphoma.* 1996;21(5-6): 443-447.
39. Chiba K, Hashino S, Izumiyama K, Toyoshima N, Suzuki S, Kurosawa M, Asaka M. Multiple osteolytic bone lesions with high serum levels of interleukin-6 and CCL chemokines in a patient with adult T cell leukemia. *Int J Lab Hematol.* 2009;31(3):368-371.
40. Chen J, Petrus M, Bryant BR, et al. Autocrine/ paracrine cytokine stimulation of leukemic cell proliferation in smoldering and chronic adult T-cell leukemia. *Blood.* 2010;116(26):5948-5956.
41. Ohshima K, Mukai Y, Shiraki H, Suzumiya J, Tashiro K, Kikuchi M. Clonal integration and expression of human T-cell lymphotropic virus type I in carriers detected by polymerase chain reaction and inverse PCR. *Am J Hematol.* 1997; 54(4):306-312.
42. Kurihara K, Harashima N, Hanabuchi S, et al. Potential immunogenicity of adult T cell leukemia cells in vivo. *Int J Cancer.* 2005;114(2):257-267.
43. Akimoto M, Kozako T, Sawada T, et al. Anti-HTLV-1 tax antibody and tax-specific cytotoxic T lymphocyte are associated with a reduction in HTLV-1 proviral load in asymptomatic carriers. *J Med Virol.* 2007;79(7):977-986.
44. Harashima N, Kurihara K, Utsunomiya A, et al. Graft-versus-Tax response in adult T-cell leukemia patients after hematopoietic stem cell transplantation. *Cancer Res.* 2004;64(1):391-399.
45. Kozako T, Arima N, Toji S, et al. Reduced frequency, diversity, and function of human T cell leukemia virus type 1-specific CD8+ T cell in adult T cell leukemia patients. *J Immunol.* 2006; 177(8):5718-5726.
46. Nakamura K, Inaba M, Sugiura K, Yoshimura T, Kwon AH, Kamiyama Y, Ikehara S. Enhancement of allogeneic hematopoietic stem cell engraftment and prevention of GVHD by intra-bone marrow bone marrow transplantation plus donor lymphocyte infusion. *Stem Cells.* 2004; 22(2):125-134.
47. Jaatinen T, Hemmoranta H, Hautaniemi S, et al. Global gene expression profile of human cord blood-derived CD133+ cells. *Stem Cells.* 2006; 24(3):631-641.
48. Herrera MB, Bruno S, Buttiglieri S, et al. Isolation and characterization of a stem cell population from adult human liver. *Stem Cells.* 2006;24(12): 2840-2850.
49. Martin-Rendon E, Hale SJ, Ryan D, et al. Transcriptional profiling of human cord blood CD133+ and cultured bone marrow mesenchymal stem cells in response to hypoxia. *Stem Cells.* 2007;25(4):1003-1012.
50. Kuruvilla JG, Troyer RM, Devi S, Akkina R. Dengue virus infection and immune response in humanized RAG2($^{-/-}$)gamma(c)($^{-/-}$) (RAG-hu) mice. *Virology.* 2007;369(1):143-152.

blood
2014 123: 346-355
doi:10.1182/blood-2013-06-508861 originally published online November 6, 2013

An animal model of adult T-cell leukemia: humanized mice with HTLV-1–specific immunity

Kenta Tezuka, Runze Xun, Mami Tei, Takaharu Ueno, Masakazu Tanaka, Norihiro Takenouchi and Jun-ichi Fujisawa

Blood (print ISSN 0006-4971, online ISSN 1528-0020), is published weekly by the American Society of Hematology, 2021 L St, NW, Suite 900, Washington DC 20036.

INTERNAL MEDICINE

□ CASE REPORT □

Human T-lymphotropic Virus Type-I (HTLV-I)-associated Myelopathy with Bulbar Palsy-type Amyotrophic Lateral Sclerosis-like Symptoms

Rina Ando, Noriko Nishikawa, Tomoaki Tsujii, Hirotaka Iwaki, Hayato Yabe, Masahiro Nagai and Masahiro Nomoto

Abstract

We herein report a case of Human T-lymphotropic virus type-I (HTLV-I)-associated myelopathy with bulbar palsy-type amyotrophic lateral sclerosis-like symptoms. A 52-year-old woman developed dyslalia at approximately 40 years of age, which slowly progressed. She presented with muscular atrophy and increased tendon reflexes of the extremities as well as bulbar palsy, from which motor neuron disease was suspected. Cerebrospinal fluid (CSF) testing revealed no abnormalities except for an elevated neopterin concentration at 143.17 pmol/mL (normal ≤30 pmol/mL). Her serum and CSF anti-HTLV-I antibody titers were also high. Intravenous infusions of methylprednisolone decreased the CSF neopterin concentration to 50.33 pmol/mL. Subsequent oral prednisolone therapy was effective in alleviating the symptoms.

Key words: HTLV-I-associated myelopathy (HAM), bulbar palsy, amyotrophic lateral sclerosis (ALS), neopterin, anti-HTLV-I antibody, steroid therapy

(Intern Med 54: 1105-1107, 2015)
(DOI: 10.2169/internalmedicine.54.3660)

Introduction

Human T-lymphotropic virus type-I (HTLV-I)-associated myelopathy (HAM) is a slowly progressive myelopathy caused by one of the human retroviruses, HTLV-I. The principal clinical manifestations of HAM are spastic paraplegia and pollakiuria (1). Cerebrospinal fluid (CSF) testing in HAM patients shows high levels of anti-HTLV-I antibody titer and neopterin (2). Immunotherapies including steroids and interferon-alpha are applied for the treatment of HAM. We herein report a case of HAM with bulbar palsy, muscular atrophy, and weakness of the upper limbs and trunk that required differentiation from bulbar palsy-type amyotrophic lateral sclerosis (ALS).

Case Report

A 52-year-old woman presented with the main complaint of dyslalia and gait disturbance. She had no remarkable medical history and did not smoke or drink alcohol. Her mother had suffered from dyslalia that developed in her 40s and she died at 70 years of age.

The patient developed dyslalia at approximately 40 years of age, which slowly progressed. Aspiration occurred at approximately 50 years of age. She visited our clinic due to frequent falls on level ground. She presented with muscular atrophy and increased tendon reflexes of the extremities as well as bulbar palsy. Because her deceased mother reportedly had similar symptoms, familial ALS was suspected and she was admitted to hospital for further evaluation.

On admission, the patient's height was 161 cm and body weight was 38.6 kg. Her vital signs were normal. She was alert and had normal cognitive function. The patient's facial muscle strength was slightly reduced in the upper part and moderately reduced in the lower part. She also had symptoms of cranial nerve disorder which included constant mouth opening, forced crying, dysphagia, dyslalia, a loss of gag reflex, tongue atrophy, fasciculation, and poor tongue protrusion. There were no other abnormal symptoms in the

Department of Neurology and Clinical Pharmacology, Ehime University Graduate School of Medicine, Japan
Received for publication July 11, 2014; Accepted for publication September 18, 2014
Correspondence to Dr. Masahiro Nagai, mnagai@m.ehime-u.ac.jp

Table. Cases of HAM Showing ALS-like Signs in the Literature

	Matsuzaki et al.[4] (n=5)	Vernant et al.[7] (n=4)	Kuroda & Sugihara[5] (n=1)	Arimura et al.[6] (n=1)
Age at onset (years)	Mean: 52.2	49–77	57	67
Course (years)	Time to abasia: Mean:5	NR	Time to death: 4.5 years	NR
Bulbar palsy	2/5	2/4	+	+
Fasciculation in tongue	3/5	NR	+	NR
Muscular atrophy in extremities	5/5	4/4	+	+
Hyperreflexia	5/5	4/4	+	+
Babinski index	4/5	NR	+	NR
Sensory disturbance	4/5	0/4	–	+
Autonomic disturbance	4/5	1/4	+/–	+
Anti-HTLV-I antibody in CSF	5/5	NR	+	NR
Anti-HTLV-I antibody in serum	5/5	4/4	+	+
Effect of steroid therapy	Improved in 2/3 treated patients	NR	NR	NR

Abbreviations: ALS: amyotrophic lateral sclerosis, CSF: cerebrospinal fluid, HAM: HTLV-I-associated myelopathy, HTLV-I: Human T-lymphotropic virus type-I, NR: not reported

cranial nerve system. Her extremities were spastic, and systemic muscular atrophy and fasciculation were observed. A manual muscle test revealed muscle weakness, predominantly in the proximal muscles, and was graded a 4 out of 5. The jaw reflex and tendon reflexes of the extremities were hyperactive. Babinski reflex was bilaterally positive and the patient had a spastic gait. Her autonomic symptoms included constipation and micturition frequency at approximately 8 to 10 times daily. She had no coordination disturbance or sensory disturbance.

Blood tests showed no significantly abnormal values in the patient's blood cell counts, blood biochemistry, markers of the auto-immune system, or various tumor markers. General CSF testing revealed no abnormal results. Magnetic resonance imaging scans of the brain and spinal cord revealed no abnormal findings. Nerve conduction studies also showed normal results. Needle electromyography showed acute neurogenic changes in the first dorsal interosseous muscle in the hand and anterior tibial muscle. SOD1 mutations were not identified in the genetic testing.

On admission, a presumptive diagnosis of familial ALS was made due to the patient's family history, the involvement of the upper and lower motor neurons in the brain stem (and upper and lower extremities), as well as a lack of sensory disturbance. However, the CSF neopterin concentration obtained on admission was elevated at 143.17 pmol/mL (normal concentrations ≤30 pmol/mL) (2) which was suggestive of an immune-mediated abnormality of the central nervous system. Therefore, testing for HTLV-I infection was conducted. The patient's serum and CSF anti-HTLV-I antibody titers were elevated (1:51,200 in serum and 1:128 in CSF). The HTLV-I proviral DNA load in the peripheral blood mononuclear cells (PBMCs) was high at 498 copies/10^4 cells [the mean±SD of HTLV-1 proviral load in asymptomatic HTLV-I carriers is 120±17 copies/10^4 PBMCs (3)]. We diagnosed this case as having HAM for the following reasons: 1) the titer of anti-HTLV-I antibody (1:128) in CSF was too high as a HTLV-I carrier with the other neurological disorders and 2) the 498 copies of HTLV-I proviral load was excessively high as a HTLV-I carrier. Matsuzaki et al. reported that ALS-like HAM patients with high HTLV-I proviral loads respond well to steroid therapy (4). Therefore, steroid therapy with intravenous infusions of methylprednisolone (1,000 mg/day) for 3 days was started and the CSF neopterin concentration rapidly fell to 50.33 pmol/mL after treatment. Subsequently, therapy with oral prednisolone was initiated at a dose of 15 mg daily. Although the dyslalia still persisted, it has improved moderately. The patient's grip strength (kg) improved from 12/13 (right/left hand) to 14/18. Her micturition frequency has reduced from approximately ten times daily to six times daily. Although amelioration of the gait disturbance has not been observed, the frequency of falls has decreased. After discharge, the dose of prednisolone was tapered. At a dose of 5 mg daily, micturition frequency increased and the CSF neopterin concentration rose to 194 pmol/mL. Hence, the dose of prednisolone was increased to 10 mg daily. Thereafter, the patient's symptoms remained stable without deterioration.

Discussion

There are several reports of HAM presenting with ALS-like symptoms as was seen in our case. In one case HAM was diagnosed on the basis of autopsy results; the subject was diagnosed as having ALS in life because of bulbar palsy and involvement of the lower and upper motor neurons in the extremities without sensory disturbance or bladder and rectal dysfunction. Several studies have reported HAM patients presenting with ALS-like features (4-9); these include a patient with bulbar palsy, systemic muscular atrophy and weakness, increased tendon reflexes of the extremities, and no sensory disturbance and a patient with bulbar palsy, systemic muscular atrophy and weakness, decreased vibratory sense in the lower legs, and impaired urination.

However, an autopsy was not performed in any of these patients. Autopsy reports on ALS-like HAM patients have described infiltration of inflammatory cells and dropout and degeneration of neural cells in the dorsal column, brain stem, cerebellum, and cerebrum in addition to the main lesions in the lateral column of the thoracic spinal cord (5, 10). Another autopsy report indicated that there were no Bunina bodies, which are unique to ALS (11).

There are two possibilities of the pathogenesis of this case: 1) HAM and ALS could have been coincidental and the inflammation process of HAM modified the ALS symptoms or 2) all of the ALS-like features were caused by HTLV-1-induced inflammation in the CNS. In the present case, the patient's symptoms began with dyslalia at approximately 40 years of age and she became unable to speak at 52 years of age. However, she was able to communicate by writing and could still walk, suggesting a slower rate of progression than that of ALS. Matsuzaki et al. reported that the average interval between onset of disease and the inability to walk is 5 years in patients with ALS-like HAM with a high HTLV-I proviral load (Table), indicating a slower rate of progression compared to typical ALS (4). Steroid therapy was not effective in ALS-like HAM patients with a low HTLV-I proviral load similar to that in asymptomatic HTLV-I carriers, whereas in ALS-like HAM patients with a high HTLV-I proviral load, steroid therapy was highly effective with efficacy almost equivalent to that seen in typical HAM patients (4, 12). The improved symptoms in our patient remained stable without deterioration by oral steroid therapy. On the basis of the high HTLV-I proviral load and the favorable response to steroid therapy, in addition to a slower progression of symptoms than that of ALS, our case was considered to be consistent with HAM presenting with ALS-like features. The measurement of neopterin and HTLV-I proviral load in HAM patients may be useful in differentiating HAM with ALS-like symptoms from ALS developing in HTLV-I carriers. Even in patients who have classical symptoms of ALS, the measurement of serum anti-HTLV-I antibody is of particular significance for differentiating HAM from ALS because half of the ALS-like HAM patients who receive steroid therapy show improvement in their symptoms.

The authors state that they have no Conflict of Interest (COI).

References

1. Osame M, Usuku K, Izumo S, et al. HTLV-I associated myelopathy, a new clinical entity. Lancet **1**: 1031-1032, 1986.
2. Nomoto M, Utatsu Y, Soejima Y, Osame M. Neopterin in cerebrospinal fluid: a useful marker for diagnosis of HTLV-I-associated myelopathy/tropical spastic paraparesis. Neurology **41**: 457, 1991.
3. Nagai M, Usuku K, Matsumoto W, et al. Analysis of HTLV-I proviral load in 202 HAM/TSP patients and 243 asymptomatic HTLV-I carriers: high proviral load strongly predisposes to HAM/TSP. J Neurovirol **4**: 586-593, 1998.
4. Matsuzaki T, Nakagawa M, Nagai M, et al. HTLV-I-associated myelopathy (HAM)/tropical spastic paraparesis (TSP) with amyotrophic lateral sclerosis-like manifestations. J Neurovirol **6**: 544-548, 2000.
5. Kuroda Y, Sugihara H. Autopsy report of HTLV-I-associated myelopathy presenting with ALS-like manifestations. J Neurol Sci Dec **106**: 199-205, 1991.
6. Arimura K, Nakagawa M, Izumo S, et al. HTLV-1-associated myelopathy (HAM) presenting with ALS-like feature. In: HTLV-I and the Nervous System. Roman G, Vernant JC, Osame M, Eds. Alan R. Liss, New York, 1989: 367-370.
7. Vernant JC, Buisson G, Bellance R, François MA, Madkaud O, Zavaro O. Pseudo-amyotrophic lateral sclerosis, peripheral neuropathy and chronic polyradiculoneuritis in patients with HTLV-1-assosiated paraplegias. In: HTLV-1 and the Nervous System. Roman G, Vernant JC, Osame M, Eds. Alan R. Liss, New York, 1989: 361-365.
8. Evans BK, Gore I, Harrell LE, Arnold T, Oh SJ. HTLV-I-associated myelopathy and polymyositis in a US native. Neurology **39**: 1572-1575, 1989.
9. Silva MT, Leite AC, Alamy AH, Chimelli L, Andrada-Serpa MJ, Araújo AQ. ALS syndrome in HTLV-I infection. Neurology **65**: 1332-1333, 2005.
10. Iwasaki Y, Sawada K, Aiba I, et al. Widespread active inflammatory lesions in a case of HTLV-I-associated myelopathy lasting 29 years. Acta Neuropathol **108**: 546-551, 2004.
11. Souza A, Tanajura D, Toledo-Cornell C, Santos S, Carvalho EM. Immunopathogenesis and neurological manifestations associated to HTLV-I infection. Rev Soc Bras Med Trop **45**: 545-552, 2012.
12. Nagai M, Tsujii T, Iwaki H, Nishikawa N, Nomoto M. Cerebrospinal fluid neopterin, but not osteopontin, is a valuable biomarker for the treatment response in patients with HTLV-I-associated myelopathy. Intern Med **52**: 2203-2208, 2013.

ARTHRITIS & RHEUMATOLOGY
Vol. 67, No. 4, April 2015, pp 1096–1106
DOI 10.1002/art.39009

Direct Infection of Primary Salivary Gland Epithelial Cells by Human T Lymphotropic Virus Type I in Patients With Sjögren's Syndrome

Hideki Nakamura,[1] Yoshiko Takahashi,[1] Tomomi Yamamoto-Fukuda,[1] Yoshiro Horai,[1] Yoshikazu Nakashima,[1] Kazuhiko Arima,[1] Tatsufumi Nakamura,[2] Takehiko Koji,[1] and Atsushi Kawakami[1]

Objective. **To investigate whether human T lymphotropic virus type I (HTLV-I) directly infects salivary gland epithelial cells (SGECs) and induces the niche of the salivary glands in patients with Sjögren's syndrome (SS).**

Methods. **SGECs were cultured with the HTLV-I–producing CD4+ T cell line HCT-5 or with Jurkat cells. Antibody arrays, immunofluorescence analysis, and enzyme-linked immunosorbent assay (ELISA) were used to determine the profiles of inflammation-related molecules, and the profiles of apoptosis-related molecules were determined by antibody array and immunofluorescence analysis. The presence of HTLV-I–related molecules was assessed by immunofluorescence analysis and in situ polymerase chain reaction. Apoptosis of SGECs was evaluated by TUNEL staining.**

Results. **Among the SGECs, 7.8 ± 1.3% (mean ± SD) were positive for HTLV-I–related proteins after 96-hour coculture with HCT-5 cells. Nuclear NF-κB p65 was also detected in 10% of the SGECs. The presence of HTLV-I proviral DNA in SGECs after coculture with HCT-5 cells was detected by in situ polymerase chain reaction. After coculture of SGECs with HCT-5, the expression of cytokines and chemokines, including soluble intercellular adhesion molecule 1, RANTES, and interferon γ–induced protein 10 kd (IP-10/CXCL10) was increased in a time-dependent manner. The expression of proapoptotic molecules (e.g., cytochrome c and Fas) and antiapoptotic molecules (e.g., Bcl-2, Heme oxygenase 2, and Hsp27) was increased in the SGECs cocultured with HCT-5, showing that apoptosis of SGECs was not detected after coculture with HCT-5 or Jurkat cells.**

Conclusion. **HTLV-I is thought to infect SGECs and alter their cellular functions. These changes may induce the niche of SS and contribute to the development of SS in anti–HTLV-I antibody–positive individuals.**

Human T lymphotropic virus type I (HTLV-I) has been reported to be involved in the pathogenesis of primary Sjögren's syndrome (SS) in endemic areas, including Nagasaki City, Japan (1–3). The extremely high prevalence of SS among patients with HTLV-I–associated myelopathy (HAM) appears to confirm a strong relationship between HTLV-I infection and SS (4–6). A previous study by our group also revealed the clinical characteristics of anti–HTLV-I antibody–positive SS patients and showed that the labial salivary glands (LSGs) of such patients are not destructible compared with the LSGs of anti–HTLV-I antibody–negative patients with SS (7). In addition, the low prevalence of ectopic germinal centers (GCs) as well as the low expression of CXCL13 in infiltrating mononuclear cells in LSGs were shown to be immunohistologic characteristics of anti–HTLV-I antibody–positive patients with SS (8).

HTLV-I preferentially infects T cells, especially CD4+ T cells, and the observations described above indicate that the T cell lineage may primarily contribute

Supported in part by a grant from the Ministry of Health, Labor, and Welfare, Japan.

[1]Hideki Nakamura, MD, PhD, Yoshiko Takahashi, MD, Tomomi Yamamoto-Fukuda, MD, PhD, Yoshiro Horai, MD, Yoshikazu Nakashima, MD, Kazuhiko Arima, MD, PhD, Takehiko Koji, PhD, Atsushi Kawakami, MD, PhD: Nagasaki University Graduate School of Biomedical Sciences, Nagasaki, Japan; [2]Tatsufumi Nakamura, MD, PhD: Nagasaki International University, Nagasaki, Japan.

Address correspondence to Hideki Nakamura, MD, PhD, Unit of Translational Medicine, Department of Immunology and Rheumatology, Nagasaki University Graduate School of Biomedical Sciences, 1-7-1 Sakamoto, Nagasaki City, Nagasaki 852-8501, Japan. E-mail: nhideki@nagasaki-u.ac.jp.

Submitted for publication April 27, 2014; accepted in revised form December 19, 2014.

to the pathogenesis of anti–HTLV-I antibody–positive SS. However, cell types other than T cells, including the human retinal pigment epithelial cell line ARPE-19 (9), and human primary fibroblast-like synoviocytes (FLS) (10) were reported to be susceptible to HTLV-I infection. In ARPE-19 cells, the expression of intercellular adhesion molecule 1 (ICAM-1) is increased by HTLV-I, and the production of granulocyte–macrophage colony-stimulating factor (GM-CSF) from FLS is induced by HTLV-I.

These observations suggested that HTLV-I may infect cell lineages other than T cells in human salivary glands and may contribute to the development of SS. In this regard, ductal epithelial cells are considered candidate cells, because various cytokines, chemokines, and apoptosis-related molecules have been shown to be expressed in these cells (1). In addition, ductal epithelial cells attract T cells into the salivary glands of patients with SS through production of interferon-γ (IFNγ)–inducible 10-kd protein (IP-10; CXCL10) and monokine induced by IFNγ (CXCL9) (11).

In the current study, we investigated whether HTLV-I infects human primary salivary gland epithelial cells (SGECs) and modulates the production of functional molecules.

PATIENTS AND METHODS

Patients. Primary SGECs were obtained from the LSGs of 15 female patients with primary SS (mean ± SD age 53.2 ± 15.4 years). In all patients, SS was diagnosed according to the revised criteria proposed by the American–European Consensus Group (12), and anti–HTLV-I antibodies were absent, as measured by chemiluminescent enzyme immunoassay.

Antibodies and reagents. Mouse anti–HTLV-I antibodies (p19, p38, and Gag) were obtained from Chemicon, and mouse anti–NF-κB p65 antibody, mouse anti–cytochrome c antibody, mouse anti-Hsp27 antibody, and rabbit anti-Fas antibody were obtained from Santa Cruz Biotechnology. Mouse anti–heme oxygenase 2 (anti–HO-2) antibody was purchased from OriGene, and rabbit anti–ICAM-1 antibody, rabbit anti–growth-related oncogene (anti-GRO)/CXCL1 antibody, anti-CCL5/RANTES antibody, and rabbit anti–IP-10/CXCL10 antibody were purchased from LifeSpan Biosciences. Rabbit anti–interleukin-8 (anti–IL-8) antibody was purchased from ABgene. Secondary antibodies, including fluorescein isothiocyanate (FITC)–conjugated donkey anti-mouse IgG and tetramethylrhodamine isothiocyanate (TRITC)–conjugated donkey anti-rabbit IgG, were purchased from Jackson ImmunoResearch. Hoechst 33258 was purchased from Sigma. A Proteome Profiler Human Cytokine Array Kit, Panel A, and a Quantikine ELISA kit for soluble ICAM-1 (sICAM-1), CXCL10/IP-10, CCR5/RANTES, CXCL1/GROα, and CXCL8/IL-8 were purchased from R&D Systems. Cy3–dUTP was purchased from GE Healthcare. Monoclonal mouse anti-human CD4, anti-human CD8, anti-human CD20cy, mouse IgG1, and monoclonal rabbit anti-human cytokeratin 8/18 antibodies were purchased from Dako.

LSG biopsy and cell culture. Each patient underwent a lower lip salivary gland biopsy under local anesthesia. Some of the specimens were stained with hematoxylin to diagnose sialadenitis, and some were used for culture of SGECs in a defined keratinocyte–serum-free medium (SFM) (Invitrogen Life Technologies) supplemented with hydrocortisone (Sigma) and bovine pituitary extract (Kurabo). In all 15 patients, the diagnosis of SS was compatible with the Chisholm and Mason scale for histologic grading of LSG biopsy tissue (13).

For the coculture of SGECs with HTLV-I–producing T cells, HCT-5 cells (which are derived from the cerebrospinal fluid cells of patients with HAM [14]), were cultured with SGECs for the designated period of time in defined keratinocyte–SFM culture medium. As a control toward HCT-5, the non–HTLV-I–infected T cell line Jurkat was cultured in RPMI 1640 medium with 10% fetal bovine serum. For the experiments described below, HCT-5 or Jurkat cells were cocultured (2:1) with SGECs at the time when the cells were seeded. Briefly, the SGECs were seeded onto sterile coverslips for immunofluorescence analysis. Next, HCT-5 cells were added 24 hours after the SGECs attached to and grew on the coverslips. For immunofluorescence analysis, the cells were stringently washed with phosphate buffered saline (PBS) to remove any remaining HCT-5 cells. Informed consent for the use of LSG biopsy samples was obtained from all 9 patients at the commencement of the study. The study was conducted with the approval of the human ethics committee at Nagasaki University Hospital.

Immunofluorescence analysis. Immunofluorescence analyses were performed as previously described (15). Briefly, SGECs cultured on 12-mm^2 coverslips were fixed in PBS containing 4% paraformaldehyde (PFA) at 4°C, followed by immersion in methanol at −20°C for 10 minutes. After fixation, the SGECs were blocked in 5% normal horse serum in PBS and then incubated with the primary antibodies for 1 hour at room temperature, followed by incubation with FITC-conjugated and TRITC-conjugated secondary antibodies and Hoechst 33258, in the dark. The SGECs were then mounted in Vectashield mounting medium (Vector) and scanned with a fluorescence microscope (BIOREVO BZ-9000; Keyence). To measure the immunofluorescence of the HCT-5 cells, fixed cells were incubated with mouse primary monoclonal antibodies as cell surface markers, followed by FITC-conjugated secondary antibody and Hoechst 33258. Control experiments were performed to confirm the isotype specificity of the secondary antibodies. Immunostaining of HCT-5 cells was performed in the same manner as that described above for SGECs.

TUNEL staining. To investigate DNA double-strand breaks in SGECs, TUNEL staining was performed as described in a previous study by our group (16). After fixation, SGECs were incubated in 4% PFA at 4°C for 15 minutes, followed by immersion in PBS with 0.5% Tween 20 and 0.2% bovine serum albumin, using a MEBSTAIN Apoptosis Kit Direct (MBL). The SGECs were then incubated with a 50-μl terminal deoxynucleotidyl transferase solution at 37°C for 1 hour. The dUTP signal as detected by FITC was captured using a BIOREVO BZ-9000 fluorescence microscope (Keyence). TRAIL was used as a positive control to show induction of apoptosis (15).

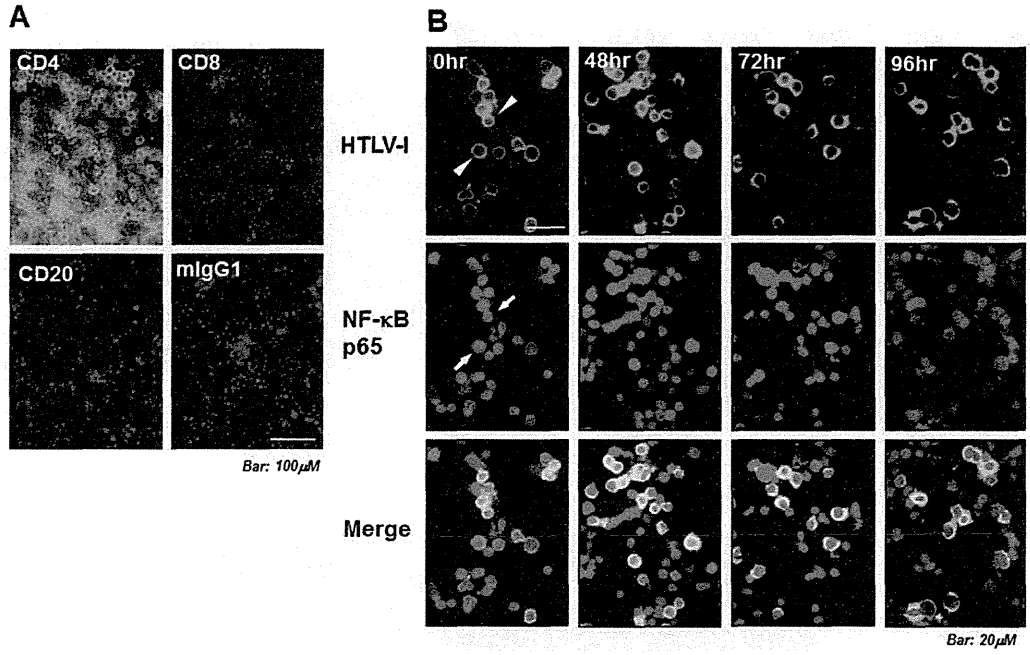

Figure 1. Characterization of the human T lymphotropic virus type I (HTLV-I)–infected HCT-5 T cell line. **A,** Phenotype of HCT-5 cells. After fixation in phosphate buffered saline containing 4% paraformaldehyde at 4°C followed by immersion in methanol at −20°C for 10 minutes, HCT-5 cells were incubated with primary antibodies (anti-CD4, anti-CD8, anti-CD20, and mouse IgG1 [mIgG1]) followed by fluorescein isothiocyanate (FITC)–conjugated secondary antibody and Hoechst 33258 (for counterstaining). **B,** Viability of HCT-5 cells. HCT-5 cells cultured for 0–96 hours in keratinocyte–serum-free medium were fixed and incubated with mouse anti–HTLV-I (p19, p28, and Gag) antibodies and rabbit anti–NF-κB p65 antibody and then incubated with FITC- and tetramethylrhodamine isothiocyanate–conjugated secondary antibodies and Hoechst 33258 (for counterstaining). **Arrowheads** indicate HTLV-I–related proteins including p19, p28, and Gag; **arrows** indicate NF-κB p65 translocation. Results are representative of 2 independent experiments with similar findings.

Cytokine detection in cocultured supernatant. A Proteome Profiler Cytokine Array system was used according to the manufacturer's instructions (R&D Systems). Briefly, after the membranes were blocked, diluted cocultured supernatant was incubated with a cocktail of biotinylated antibodies for 1 hour. The mixture of cytokines, chemokines, and antibodies was then incubated for 2 hours using this array system, combined with an immobilized antibody on the membrane. For the detection of cytokines and chemokines, chemiluminescent reagents were used after incubation with streptavidin–horseradish peroxidase (HRP).

Analysis of apoptosis in cocultured lysate. A Proteome Profiler Apoptosis Antibody Array system was used to analyze apoptosis pathways, according to the manufacturer's instructions (R&D Systems). Briefly, diluted cocultured cellular extracts were incubated on membranes for 2 hours after the membranes were blocked for 1 hour. After a 2-hour incubation, a cocktail of biotinylated antibodies was added to the membranes and incubated for 1 hour. Chemiluminescent reagents were then used after incubation with streptavidin–HRP for 30 minutes.

Cytokine and chemokine enzyme-linked immunosorbent assays (ELISAs). The levels of sICAM-1, CXCL10/IP-10, CCR5/RANTES, CXCL1/GROα, and CXCL8/IL-8 (all from R&D Systems) were measured by ELISA, according to the manufacturer's instructions. Briefly, the assigned volume of cell culture supernatant, standard, or control was added to an ELISA well and incubated for the indicated periods of time. After the wells were washed and decanted 3 times, each conjugate was added to a well and incubated for 1 hour at 4°C. After the washing process, substrate solution was added to each well and incubated for 15 minutes. After the addition of stop solution, optical density at 450 nm was measured.

In situ PCR of HTLV-I proviral DNA in cocultured SGECs. Initially, SGECs (alone or in coculture with HCT-5) were fixed in 0.5 ml Carnoy's fixative for 20 minutes at room temperature, followed by washing with 0.5 ml 70% ethanol for 15 minutes at room temperature on type I collagen–coated 12-mm^2 coverslips. After treatment with prewarmed protein kinase (1 μg/ml) at 37°C for 15 minutes and 3 washes with PBS, the SGECs were fixed with 4% PFA/PBS for 5 minutes and then were immersed in 50% formamide/2× saline–sodium citrate buffer at 4°C overnight. After being washed with deuterium-depleted water 3 times for 5 minutes each time, the cells were mixed with an amplification cocktail that consisted of a final concentration of 1× PCR buffer, 1 μg/ml forward primer (5′-CGGATACCCAGTCTACGTGT-3′), 1 μg/ml reverse primer (5′-GAGCCGATAACGCGTCC-3′) (17), 0.2 m*M* dNTP, 2.5 m*M* $MgCl_2$, 1 μ*M* Cy3–dUTP, and distilled water without DNA polymerase, and then boiled for 10 minutes.

Application of these primer sets was previously described

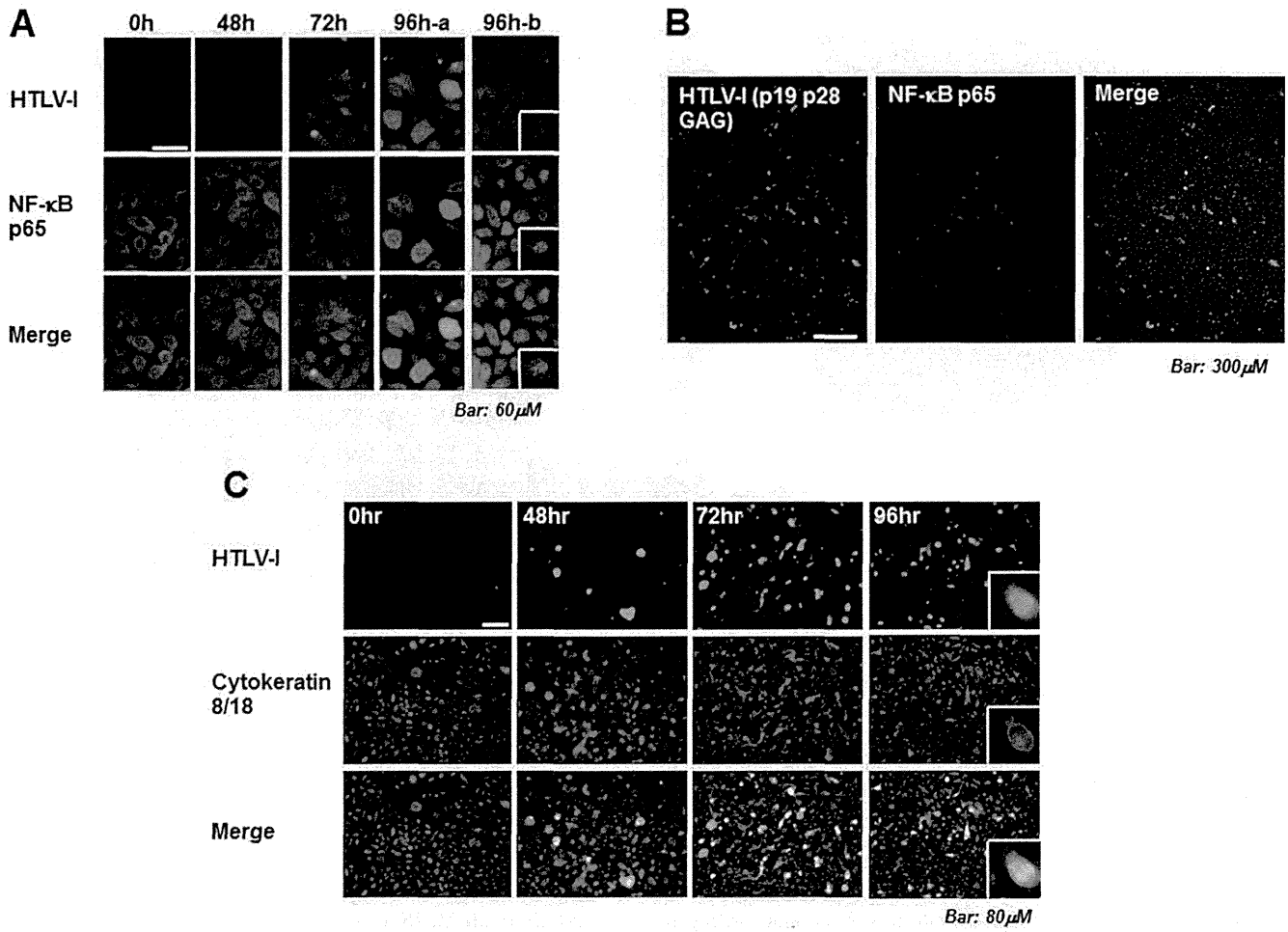

Figure 2. Detection of HTLV-I–related molecules in cocultured salivary gland epithelial cells (SGECs). **A,** Presence of HTLV-I proteins (p19, p28, and Gag), as determined by immunofluorescence analysis. SGECs cocultured for 0–96 hours were fixed in phosphate buffered saline containing 4% paraformaldehyde at 4°C followed by immersion in methanol at −20°C for 10 minutes. The SGECs were initially incubated with anti–HTLV-I antibody and NF-κB p65 followed by FITC- and tetramethylrhodamine isothiocyanate (TRITC)–conjugated secondary antibodies, respectively, and Hoechst 33258 for counterstaining. To contrast the increased expression of HTLV-I proteins without NF-κB translocation (96h-a), translocation of NF-κB is shown (96h-b). **B,** Low-magnification view of cocultured SGECs and HCT-5 cells at 96 hours, showing positive staining for HTLV-I in ~10% of SGECs. **C,** Frequency of HTLV-I–infected SGECs during 0–96-hour coculture, as determined by immunofluorescence analysis. SGECs were initially incubated with anti–HTLV-I antibody and anticytokeratin 8/18 antibody (to distinguish HTLV-I–infected SGECs from HCT-5 cells) followed by FITC- and TRITC-conjugated secondary antibodies, respectively, and Hoechst 33258 for counterstaining. In the merged view, yellow indicates HTLV-I–infected SGECs, and green indicates HCT-5 cells. Results are representative of 3 independent experiments. **Insets** in *A* and *C* show representative cells in each panel. See Figure 1 for other definitions.

in a study by Matsuoka et al, in which the positions of the forward and reverse primers were 7,358–7,377 and 7,516–7,494 of the HTLV-I pX region, respectively (17). After KAPA2G Fast DNA Polymerase complete amplification cocktail (Kapa Biosystems) was added to the SGECs and they were sealed with clear rubber covers, then the coverslips were placed in a thermocycler for in situ PCR (Hybaid). The details of the in situ PCR were as follows: each block was heated at 92°C for 3 minutes, 5 PCR cycles were performed (92°C for 1 minute, 47°C for 1 minute, and 70°C for 2 minutes), and the block was then held at 70°C for 5 minutes. The reacted coverslips were then washed 4 times with 2× saline–sodium citrate at 37°C for 15 minutes, followed by 2 washes with 0.5× saline–sodium citrate at 45°C for 15 minutes. After the coverslips were reacted with PBS once and covered with Vectashield mounting medium, SGECs were visualized using fluorochrome with a BIOREVO BZ-9000 fluorescence microscope.

Statistical analysis. Differences in ELISA results were analyzed using Student's *t*-test. *P* values less than 0.05 were considered significant.

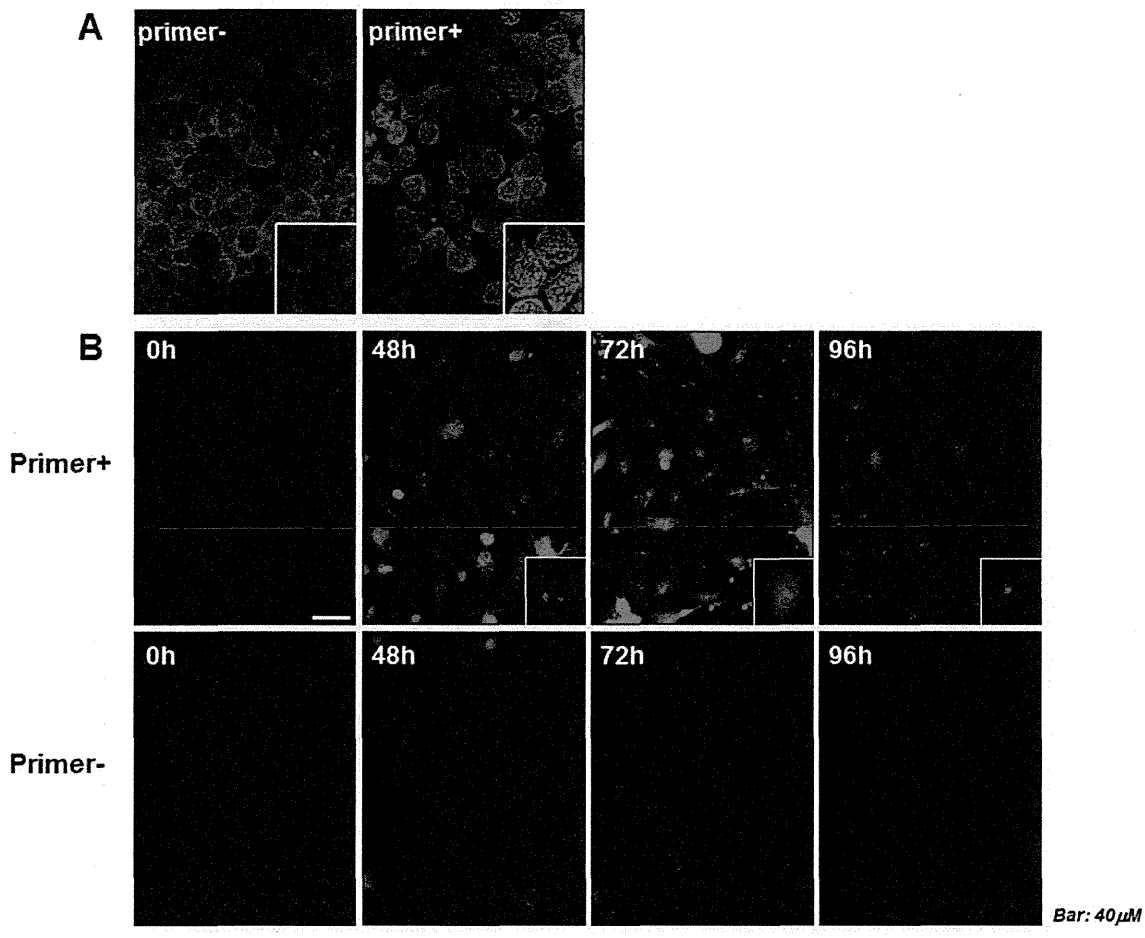

Figure 3. Detection of human T lymphotropic virus type I (HTLV-I) proviral DNA by in situ polymerase chain reaction (PCR). **A,** HTLV-I was detected in HCT-5 cells as a positive control. HCT-5 cells were treated with 1 μg/ml of protein kinase, and 5 cycles of in situ PCR were performed. Detected HTLV-I proviral DNA is shown as a granular pattern signal. **B,** Fixed salivary gland epithelial cells were treated with 1 μg/ml of protein kinase, and 5 cycles of in situ PCR were then performed in the presence or absence of primers for the HTLV-I pX region. Detected signal is indicated as the appearance of dots in the nucleus of salivary gland epithelial cells. Results are representative of 2 independent experiments with similar findings. **Insets** show representative cells in each panel.

RESULTS

Phenotype and viability of HCT-5 cells. The HCT-5 cells used for coculture with SGECs showed the CD4+ phenotype (Figure 1A), with no staining for CD8 or CD20. The HCT-5 cells cultured for 0–96 hours in keratinocyte–SFM were viable, with translocation of nuclear NF-κB into SGECs after coculture (Figure 1B).

Detection of HTLV-I–related proteins in SGECs during coculture. After coculture of SGECs and HCT-5 cells, immunofluorescence analysis showed clear signals for HTLV-I proteins p19, p28, and Gag at 72–96 hours (Figure 2A). At 96 hours, ~10% of the SGECs cocultured with HCT-5 cells showed HTLV-I–positive staining at low magnification (Figure 2B). Nuclear NF-κB p65 was also detected in 10% of the SGECs after coculture (Figures 2A and B). To distinguish HTLV-I–infected SGECs from HCT-5 cells, SGECs were stained with cytokeratin 8/18 antibodies (Figure 2C), which was reported to be one of markers for SGECs (18). In merged view (yellow signal), the mean ± SEM frequency of HTLV-I–infected SGECs was calculated as 7.8 ± 1.3%, and the remaining HCT-5 cells (green signal) were observed during coculture for 48–96 hours.

Detection of HTLV-I DNA in SGECs by in situ PCR. To clarify whether HTLV-I infected SGECs during coculture with HCT-5 cells and investigate the details, we determined HTLV-I DNA expression. As a positive control, HTLV-I proviral DNA was detected in HCT-5 cells (Figure 3A).

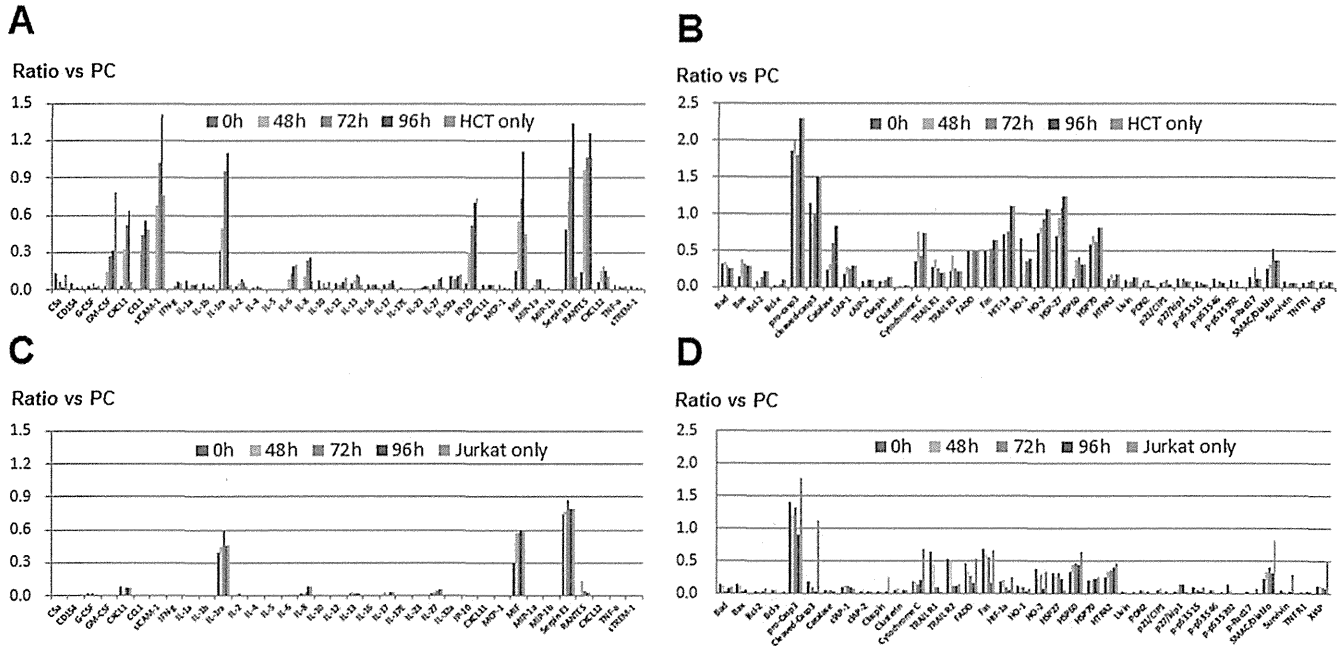

Figure 4. Expression of inflammation-related molecules and apoptosis-related molecules. **A** and **C,** Expression of inflammation-related molecules in supernatant of salivary gland epithelial cells (SGECs) cocultured with HCT-5 cells (**A**) or Jurkat cells (**C**). The semiquantitative concentrations of each molecule in culture medium (i.e., keratinocyte–serum-free medium) after coculture with HCT-5 cells or Jurkat cells is shown. "HCT-5 only" and Jurkat only" indicate the culture supernatant for HCT-5 cells and Jurkat cells, respectively. **B** and **D,** Expression of apoptosis-related molecules in lysate of SGECs cocultured with HCT-5 cells (**B**) or Jurkat cells (**D**). The semiquantitative concentration of each molecule in recovered SGEC lysate after coculture with HCT-5 cells or Jurkat cells is shown. Results are representative of 2 independent experiments with similar findings. PC = positive control.

During coculture, amplified HTLV-I DNA was observed in the nucleus of SGECs in the presence of primer at 48 hours of coculture with HCT-5 cells (Figure 3B). The strongest HTLV-I DNA signal was observed in the presence of primer at 72 hours of coculture.

Increased expression of inflammation-related molecules and apoptosis-related molecules in cocultured SGECs. As shown in Figure 4A, the expression of GM-CSF, CXCL1/GROα, CCL1, sICAM-1, IL-1 receptor antagonist (IL-1Ra), IL-6, IL-8, CXCL10/IP-10, macrophage migration inhibitory factor (MIF), serpin E1, and CCR5/RANTES in cocultured HCT-5/SGEC supernatant increased in a time-dependent manner. The results of apoptosis analysis using SGEC lysate cocultured with HCT-5 are shown in Figure 4B. The responses of proapoptotic molecules including procaspase 3, cytochrome c, and Fas in the lysate were slightly increased after coculture of SGECs with HCT-5 cells. The signals for antiapoptotic molecules including Bcl-2, HO-2, Hsp27, or second mitochondria-derived activator of caspases (SMAC)/Diablo were also up-regulated after coculture.

As shown in Figures 4C and D, the expression of IL-1Ra, MIF, and serpin E1 was increased after coculture of SGECs with Jurkat cells; however, the increase was not time dependent (Figure 4C). In contrast to the results of coculture of SGECs with HCT-5, expression of other molecules including GM-CSF, CXCL1/GROα, CCL1, sICAM-1, IL-6, IL-8, and CXCL10/IP-10 was not increased following coculture of SGECs with Jurkat cells. The results of the apoptosis analysis using SGEC lysate cocultured with Jurkat cells are shown in Figure 4D. Although expression of procaspase 3 and SMAC/Diablo was similar to that observed in HCT-5/SGEC coculture, expression of cytochrome c, Fas, Bcl-2, HO-2 and Hsp27 was not up-regulated after coculture of SGECs with Jurkat cells.

The data derived from analyses using a cytokine array system and an apoptosis antibody array system were confirmed by immunofluorescence analysis and ELISA. Immunofluorescence analysis showed increased cytoplasmic expression of ICAM-1, CXCL1, RANTES, IL-8, and IP-10 (Figure 5A), with augmentation of the signals for HTLV-I p19, p28, and Gag in SGECs after